

# Quark-meson-diquark model for two-color QCD

Nils Strodthoff,<sup>1,\*</sup> Bernd-Jochen Schaefer,<sup>2,3,†</sup> and Lorenz von Smekal<sup>1,‡</sup>

<sup>1</sup>*Institut für Kernphysik, Technische Universität Darmstadt, D-64289 Darmstadt, Germany*

<sup>2</sup>*Institut für Physik, Karl-Franzens-Universität Graz, A-8010 Graz, Austria*

<sup>3</sup>*Institut für Theoretische Physik, Justus-Liebig-Universität Gießen, D-35392 Gießen, Germany*

We introduce a two-flavor quark-meson-diquark model for two-color QCD and its extensions to include gauge-field dynamics as described by the Polyakov loop. Grand potential and phase structure are being studied both in mean-field approximation and with the functional renormalization group. The model provides an explicit example for the importance of baryonic degrees of freedom: When they are omitted, the phase diagram closely resembles that of the corresponding (Polyakov)-quark-meson models for QCD, in particular including their critical endpoint. In order to reproduce the well established main features based on the symmetries and breaking patterns of two-color QCD, however, they must be included and there is no critical endpoint. The competing dynamics of collective mesonic and baryonic fluctuations is well described by the functional renormalization group equation in lowest order derivative expansion for the effective potential which we solve numerically on a two-dimensional grid in field space.

PACS numbers: 12.38.Aw, 11.10.Wx, 11.30.Rd, 12.38.Gc

## I. INTRODUCTION

The phase diagram of Quantum Chromodynamics (QCD) is subject to enormous international research campaigns [1, 2]. In order to understand its main characteristic features such as the different phases of strongly interacting matter, the nature of the transitions between them, the existence and locations of critical points or perhaps approximate triple points and even multicritical points, it has proven to be very useful to deform QCD by not only varying the individual quarks' masses but also the numbers of their different flavors and colors. An important example is the limit of infinitely many colors  $N_c$  which inspired many qualitative descriptions of the QCD phase diagram [3–5]. One interesting aspect of this limit is that the baryon density becomes an order parameter for  $N_c \rightarrow \infty$ , in particular, also when the number of flavors  $N_f$  grows along with  $N_c$ , *i.e.* for  $N_f/N_c$  held fixed. In this paper we study two-color QCD, which shares this aspect of the large- $N$  limit, here with  $N_c = N_f = 2$ . If one accepts that the phases of many-color QCD with  $N_c \sim N_f \rightarrow \infty$  have a bearing on the real world, it might therefore not be absurd, with due appreciation of all differences, to consider  $N_c = N_f = 2$  either.

Quantum Chromodynamics with two colors (QC<sub>2</sub>D) has been well studied for many years within chiral effective field theory and random matrix theory [6–14], in lattice simulations [15–22], and the Nambu–Jona-Lasinio model [23–32]. In this paper we formulate a Polyakov-quark-meson-diquark (PQMD) Model for studying the phase diagram of QC<sub>2</sub>D with the functional renormalization group, including fluctuations due to collective excitations.

The most important differences between two and three colors follow from the special property of the  $SU(2)$  gauge group of QC<sub>2</sub>D: Its representations are either pseudo-real or real which leads to an antiunitary symmetry in the Dirac operator [7]. As a result, the fermion determinant remains real for non-vanishing baryon or quark chemical potential,  $\mu \neq 0$ , as it does for adjoint quarks in any-color QCD, or in the  $G_2$  gauge theory with fundamental fermions also, for example. Thus, for an even number of degenerate fundamental quark flavors in QC<sub>2</sub>D there is *no fermion-sign problem* and the phase diagram is amenable to lattice Monte-Carlo simulations. Symmetry considerations, lattice simulations and non-perturbative functional continuum methods together should therefore allow us to understand the phase diagram of this theory completely. A combined effort towards this goal will be very worthwhile in particular because it will help to bring the functional continuum methods to a level at which they can reliably be applied, with the necessary adjustments, also to real QCD where lattice simulations suffer from the infamous fermion-sign problem [33].

Another consequence of the pseudo-reality is the Pauli-Gürsey symmetry which allows to combine quarks and charge-conjugated antiquarks into enlarged flavor multiplets. As a result, for vanishing chemical potential and quark mass,  $\mu = m_q = 0$ , the usual  $SU(N_f) \times SU(N_f) \times U(1)_B$  chiral and baryon number symmetries are replaced by an extended  $SU(2N_f)$  flavor symmetry which is (spontaneously) broken by a (dynamical) Dirac mass down to the  $(2N_f + 1)N_f$  dimensional compact symplectic group  $Sp(N_f)$ . For  $N_f = 2$  the extended flavor symmetry group  $SU(4)$  and its  $Sp(2)$  subgroup are locally isomorphic to the rotation groups  $SO(6)$  and  $SO(5)$ , respectively. The coset is given by  $S^5$ , the unit sphere in six dimensions, and a spontaneously generated Dirac mass will lead to five Goldstone bosons, the three pions plus a scalar diquark-antidiquark pair.

Moreover, for  $N_c = 2$  these color-singlet scalar di-

\* nstrodth@theorie.ikp.physik.tu-darmstadt.de

† bernd-jochen.schaefer@uni-graz.at

‡ lorenz.smekal@physik.tu-darmstadt.de

quarks play a dual role as bosonic baryons at the same time. While this thus represents the perhaps most important difference as compared to the real world, it also makes it much easier to investigate the effects of baryonic degrees of freedom on the phase diagram in functional approaches. In that sense our model can be considered as a first step towards their inclusion in a ‘quark-meson-baryon’ model for real QCD with three colors.

For the same reason our model of  $QC_2D$  provides a relativistic analogue of the BEC-BCS crossover in ultracold fermionic quantum-gases, which has also been described successfully with functional renormalization group methods [34, 35]. In contrast to non-relativistic models of the BEC-BCS crossover, an interesting additional constraint thereby arises from the Silver Blaze property [36]: When a relativistic chemical potential  $\mu$  is coupled to degrees of freedom with a mass gap  $\Delta$ , at zero temperature, the partition function and hence thermodynamic observables must actually remain independent of the chemical potential as long as  $\mu < \Delta$ . We will see that it is not trivial, in general, to implement this constraint in non-perturbative functional renormalization group studies, and that it can provide valuable extra information to devise intelligent truncations.

Our main interest here, however, is to explicitly demonstrate the impact of baryonic degrees of freedom on the phase diagram by comparing the purely mesonic model, representative of typical three-color QCD model calculations, to the full quark-meson-diquark model.

For this comparison we argue that it is more appropriate to think of the vacuum diquark mass as the baryon mass  $m_B$  rather than the pion mass  $m_\pi$ . In  $QC_2D$  with its extended flavor symmetry they are the same, but the essential aspect of this assignment is that a continuous phase transition at zero temperature occurs at a critical quark chemical potential  $\mu_c = m_B/N_c$ . Except for the scale separation between  $m_\pi$  and  $m_B$  in the real world, this transition can then be thought to correspond to the liquid-gas transition of nuclear matter in QCD with three colors which is of first order, involves the binding energy, and thus occurs somewhat below  $\mu = m_B/N_c$ .

As temperature increases the liquid gas transition ends, turning into a crossover with continuously varying but nevertheless probably still relatively abruptly increasing baryon density along some narrow region. This rapid increase is generally expected to lead to the strong chemical-potential dependence of the chemical freeze-out line observed in heavy ion collisions at center-of-mass energies below about 10 GeV per nucleon pair, the baryonic freeze-out [37, 38]. One might conclude that the phase transition line for diquark condensation, where a rapidly increasing baryon density spontaneously develops, would be the origin of a corresponding baryonic freeze-out line in two-color QCD, with  $N_c = N_f = 2$  arguably not necessarily further from reality than the large  $N_c$  limits. As in the latter, one might then even identify a two-color version of quarkyonic matter [3, 4, 21, 28].

Finally, we would like to point out that our model,

the functional renormalization group equations and the techniques to solve them have a broad scope of applications beyond two-color QCD. One example is QCD with two light flavors at finite isospin chemical potential, which has been studied with the NJL model in mean-field plus random phase approximation (RPA) [39, 40]. There is a precise equivalence between the corresponding quark-meson model with isospin chemical potential and our quark-meson-diquark model of two-color QCD. Besides changing  $N_c$  this merely involves reducing the number of would-be Goldstone bosons from five to three again, retaining only one of our degenerate pions, and reinterpreting the diquarks as the charged pions with isospin chemical potential [41]. Similar models are also studied in the context of color superconductivity [42–44]. The capacity to numerically solve functional renormalization group equations on higher dimensional grids in field space is generally useful for competing symmetries, as in a quark-meson model study of the axial anomaly with scale dependent ’t Hooft couplings, for example [45].

The outline of this paper is as follows: In Sec. II we review the general features of  $QC_2D$  such as its enlarged flavor symmetry and the possible symmetry breaking patterns in some more detail. Based on these symmetry considerations we then construct the Polyakov-loop extended quark-meson-diquark Lagrangian for  $QC_2D$ . In the next section, Sec. III, we derive the thermodynamic potential of the (P)QMD model in mean-field approximation, discuss so-called vacuum contributions, the Silver Blaze property and the relevance of pole versus screening masses for mesons and diquarks. The functional renormalization group flow equations for the effective potential in leading-order derivative expansion are derived in Sec. IV. In this section we also calculate critical exponents which are consistent with the expected symmetry breaking pattern, investigate in how far mean-field results are modified by fluctuations, and give a transparent illustration of the importance of baryonic degrees of freedom for the phase diagram. As a byproduct we note that starting from a tricritical point, a region of first-order transition limiting the diquark condensation phase at larger chemical potentials as predicted from chiral perturbation theory at next-to-leading order [9], is also observed in the QMD model at the mean-field level. This first-order transition turns out to be a mean-field artifact, however. It is washed out by the fluctuations, and there is no sign of a tricritical point left, once the thermodynamic potential is obtained from its functional renormalization group flow. We draw our conclusions and present an outlook in Sec. V. Technical details can be found in several appendices.

## II. FLAVOR SYMMETRIES IN $QC_2D$

We begin this section with a short review of the extended flavor symmetries of  $QC_2D$  due to its Pauli-Gürsey symmetry, and the associated symmetry breaking

patterns. We then discuss a qualitative phase diagram for two-flavor QC<sub>2</sub>D and construct the quark-meson-diquark (QMD) model by a suitable vector coupling of quark bilinears to meson and diquark fields.

### A. Extended flavor symmetries and symmetry breaking patterns

As all half-odd integer representations of  $SU(2)$ , its fundamental representation is pseudoreal, which means that it is isomorphic to its complex conjugate representation with the isometry given by  $S = i\sigma_2$ ,  $S^2 = -1$ .<sup>1</sup> Therefore, charge conjugation of the gauge fields in QC<sub>2</sub>D can be undone by the constant  $SU(2)$  gauge transformation  $S = i\sigma_2$ . From now on we will use  $T^a = \sigma^a/2$  for the color generators, with

$$T^{aT} = T^{a*} = -ST^a S^{-1}, \quad (1)$$

and reserve  $\sigma_i$  ( $\tau_i$ ) for the Pauli matrices in spinor (flavor) space. Together with the charge conjugation matrix  $C$  in spinor space, likewise with  $C^2 = -1$ , and complex conjugation denoted by  $K$  one then defines an antiunitary symmetry  $T = SCK$  with  $T^2 = +1$  (in a real color representation with  $S^2 = +1$ , one has  $T^2 = -1$ , correspondingly). This leads to the classification of the Dirac operator by the Dyson index  $\beta$  of random matrix theory [6, 7], with  $\beta = 1$  for fermions in the pseudoreal fundamental color representation of QC<sub>2</sub>D (or  $\beta = 4$  in the real color representations of  $SU(N)/Z_N$  or  $G_2$ ).

Following [7], we start from the standard kinetic part of the Euclidean QC<sub>2</sub>D Lagrangian, in the chiral basis,

$$\mathcal{L}_{\text{kin}} = \bar{\psi} \not{D} \psi = \psi_L^\dagger i\sigma_\mu D_\mu \psi_L - \psi_R^\dagger i\sigma_\mu^\dagger D_\mu \psi_R, \quad (2)$$

with hermitian  $\gamma$ -matrices,  $\sigma_\mu = (-i, \vec{\sigma})$ , and  $\psi_{R/L}$ ,  $\psi_{R/L}^*$  as independent Grassmann variables with  $\psi_{R/L}^\dagger \equiv \psi_{R/L}^{*T}$ . The covariant derivative is  $D_\mu = \partial_\mu + iA_\mu$ , and the coupling is absorbed in the gauge fields  $A_\mu = A_\mu^a T^a$ .

The two terms in (2) get interchanged under the antiunitary symmetry  $T$ . If we apply it only to the second term, say, by using  $(-i\sigma_2)$  for the chiral  $R$ -component of the charge conjugation matrix  $C$ , *i.e.*, changing variables to  $\tilde{\psi}_R = -i\sigma_2 S \psi_R^*$  and  $\tilde{\psi}_R^* = -i\sigma_2 S \psi_R$ , we can therefore reexpress

$$\mathcal{L}_{\text{kin}} = \Psi^\dagger i\sigma^\mu D_\mu \Psi \quad (3)$$

in terms of the  $2N_f$  4-dimensional spinors  $\Psi = (\psi_L, \tilde{\psi}_R)^T$  and  $\Psi^\dagger = (\psi_L^\dagger, \tilde{\psi}_R^\dagger)$ . Because it is now block diagonal, the  $SU(2N_f)$  symmetry in the space combining flavor and

transformed chiral components is manifest in this form. With the same transformation of variables the quarks' Dirac-mass term becomes

$$m\bar{\psi}\psi = \frac{m}{2} (\Psi^T i\sigma_2 S \Sigma_0 \Psi - \Psi^{*T} i\sigma_2 S \Sigma_0 \Psi^*), \quad (4)$$

where the symplectic matrix

$$\Sigma_0 = \begin{pmatrix} 0 & \mathbb{1}_{N_f} \\ -\mathbb{1}_{N_f} & 0 \end{pmatrix} \quad (5)$$

acts in the  $2N_f$ -dimensional extended flavor space. An explicit(dynamical) Dirac mass therefore explicitly(spontaneously) breaks the original  $SU(2N_f)$  down to the compact symplectic group  $Sp(N_f)$ , sometimes also referred to as  $USp(2N_f)$  reflecting the fact that it is the intersection of the unitary  $U(2N_f)$  and the symplectic  $Sp(2N_f, \mathbb{C})$ , the invariance group of  $\Sigma_0$  as bilinear form on complex  $2N_f$ -vectors.

For  $N_f = 2$  flavors the enlarged flavor symmetry group of QC<sub>2</sub>D is  $SU(4)$ , not  $U(4)$  because of the axial anomaly, it replaces the usual chiral and baryon number symmetries  $SU(2)_L \times SU(2)_R \times U(1)_B$ . Just as this extended flavor  $SU(4)$  shares its 15 dimensional Lie algebra with the group of rotations in 6 dimensions,  $SO(6)$ , its  $Sp(2)$  subgroup leaving the Dirac-mass term invariant has the 10 dimensional Lie algebra of  $SO(5)$  (in fact they are both the universal covers of the respective rotation groups).

Our brief review of the QC<sub>2</sub>D symmetries so far holds for vanishing chemical potential. For  $\mu \neq 0$  but  $m = 0$ , the  $SU(2N_f)$  symmetry is broken explicitly by  $\mu\bar{\psi}\gamma_0\psi$  to  $SU(N_f)_L \times SU(N_f)_R \times U(1)$ . This is also easy to see, from Eqs. (2), (3), as it amounts to introducing the term  $\mu\bar{\psi}\gamma_0\psi = \mu\Psi^\dagger B_0 \Psi$  with [7]

$$B_0 = -\gamma_0 \Sigma_0 = \begin{pmatrix} \mathbb{1}_{N_f} & 0 \\ 0 & -\mathbb{1}_{N_f} \end{pmatrix}. \quad (6)$$

For  $N_f = 2$ , in terms of the rotation groups, this symmetry breaking pattern is locally the same as  $SO(6) \rightarrow SO(4) \times SO(2)$ .

When both  $\mu$  and  $m$  are non-zero, the unbroken flavor symmetry is of course given by the common subgroup  $SU(2)_V \times U(1)$  of the two limiting cases  $\mu \rightarrow 0$ ,  $m \neq 0$  or  $m \rightarrow 0$ ,  $\mu \neq 0$  discussed above. Whether, as an approximate symmetry, it is more like the  $Sp(2) \simeq SO(5)$  or like the  $SU(2)_L \times SU(2)_R \times U(1) \simeq SO(4) \times SO(2)$ , naturally depends on the relative sizes of Dirac mass  $m$  and quark chemical potential  $\mu$ .

More precisely, it is an exact result of chiral effective field theory [6, 7], that for baryon chemical potential  $\mu_B = 2\mu < m_\pi$  the approximate chiral symmetry breaking pattern remains that of  $\mu = 0$  and the vacuum alignment is  $\langle \bar{q}q \rangle$ -like with an approximate  $Sp(2) \simeq SO(5)$  if  $m$  is sufficiently small, while (at zero temperature) for  $\mu_B = 2\mu > m_\pi$  a diquark condensate develops and the vacuum alignment starts rotating from being  $\langle \bar{q}q \rangle$ -like to becoming more and more  $\langle qq \rangle$ -like as  $\mu$  is further increased. The chiral condensate then rapidly decreases, chiral symmetry appears to get restored but the

<sup>1</sup> The irreducible representations of the proper rotations are real which means their complex conjugates are obtained from isometries  $S$  with  $S^2 = +1$ , just as those of the adjoint groups  $SU(N)/Z_N$  or most of the exceptional Lie groups such as  $G_2$ .

increasing chemical potential reduces it to the approximate  $SU(2)_L \times SU(2)_R \simeq SO(4)$  again. It is not the full flavor symmetry of the  $\mu \neq 0$ ,  $m = 0$  case discussed above because we have entered the diquark-condensation phase with spontaneous baryon-number breaking, corresponding to superfluidity of the bosonic baryons.

Another exact result is that, at zero temperature and for  $\mu_B < m_\pi$ , the onset of baryon condensation, the baryon density remains zero and the thermodynamic observables must be independent of  $\mu$ . Because this is far from obvious to verify explicitly in actual calculations, it has been named the Silver Blaze Problem [36]. In order to be able to excite any states at zero temperature, and with a gap in the spectrum, the relativistic chemical potential needs to be increased beyond the mass gap in the correlations to which it couples. Here, with a continuous zero-temperature transition at  $\mu_B = m_\pi$  this gap is simply given by the baryon mass in vacuum which because of the extended flavor symmetry in QC<sub>2</sub>D coincides with the pion mass,  $m_B = m_\pi$ . This latter property is of course special to  $N_c = 2$ . The Silver Blaze property will hold, as it does here, up to a quark chemical potential of the order of  $m_B/N_c$  (reduced by  $1/N_c$  of the binding energy per nucleon when the transition is of first order), in general, however.

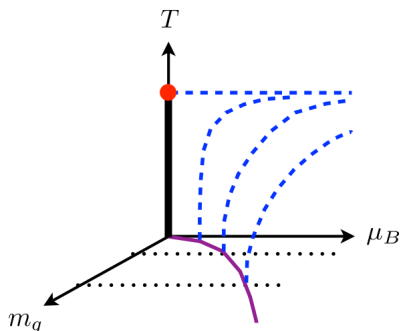


FIG. 1. Schematic phase diagram for QC<sub>2</sub>D in the parameter space of temperature  $T$ , quark mass  $m_q$  and baryon chemical potential  $\mu_B$ .

At finite temperature, a qualitative picture emerges for the phase diagram as sketched in Fig. 1. The solid line in the  $T = 0$  plane there represents the continuous zero-temperature transition with diquark condensation which is of mean-field type. Because the quark mass  $m_q$  scales quadratically with the pion mass, it will occur along a parabola  $m_q \propto \mu_B^2$ . The thick dashed lines represent the corresponding second-order transitions at finite temperature in fixed  $m_q$  planes of the  $O(2)$  universality. The thick line along the temperature axis is the magnetic first-order transition in the  $\mu_B = 0$  plane which probably ends in a multi-critical point. When viewed in the  $\mu_B = 0$  plane, this is the critical endpoint in the  $O(6)$  universality class for the chiral phase transition in QC<sub>2</sub>D with its extended  $SU(4)$  flavor symmetry. In the  $m_q = 0$  plane, the vacuum alignment will always be  $\langle qq \rangle$ -like, for no-matter-how-small  $\mu > 0$ . Therefore, in this plane one

only has the second-order  $O(2)$  line which might end in the same point making it multi-critical.

## B. Quark-meson-diquark model Lagrangian

The starting point of our model construction is the flavor structure of the standard chiral condensate and the quark mass term which is of the form  $\Psi^T \Sigma_0 \Psi$ . It therefore transforms under the full flavor  $SU(4)$  according to the six-dimensional antisymmetric representation in the decomposition  $4 \otimes 4 = 10 \oplus 6$ .

The other components belonging to the same multiplet are obtained from transformations

$$\Psi \rightarrow U\Psi, \quad U = \exp(i\theta^a X^a) \in SU(4)/Sp(2). \quad (7)$$

Then,  $\Psi^T \Sigma_0 \Psi \rightarrow \Psi^T \Sigma \Psi$ , where, from Cartan's immersion theorem, the whole coset  $SU(4)/Sp(2) \cong S^5$  is obtained in this way via  $\Sigma \equiv U^T \Sigma_0 U$ . The coset elements  $\Sigma$  are in turn parametrized by six-dimensional unit vectors  $\vec{n}$  as  $\Sigma = \vec{n} \vec{\Sigma}$ , with  $\Sigma_i^\dagger \Sigma_j + \Sigma_j^\dagger \Sigma_i = 2\delta_{ij}$  and  $\vec{\Sigma} = (\Sigma_0, i\Sigma_0 X^a)$  such that  $X^a$ ,  $a = 1 \dots 5$ , form a basis for the coset generators [11]. Thus, one verifies explicitly that the vector  $\Psi^T \vec{\Sigma} \Psi$  transforms as a (complex) six-dimensional vector under  $SO(6)$ .

A locally  $SU(2)_c$  invariant linear sigma model Lagrangian can therefore be defined by coupling the real  $SO(6)$  vector of quark bilinears ( $\Psi^T \vec{\Sigma} \Psi + \text{h.c.}$ ) to a vector of mesonic fields  $\vec{\phi} = (\sigma, \vec{\pi}, \text{Re } \Delta, \text{Im } \Delta)^T$  formed by the scalar  $\sigma$  meson, the pseudoscalar pions  $\vec{\pi}$  and the scalar diquark-antidiquark pair  $\Delta$ . This yields the Lagrangian (now including color and spinor components again),

$$\begin{aligned} \mathcal{L}_\sigma = & \Psi^\dagger i\sigma^\mu D_\mu \Psi + \frac{g}{2} (\Psi^T i\sigma_2 S \vec{\Sigma} \Psi - \Psi^{*T} i\sigma_2 S \vec{\Sigma} \Psi^*) \vec{\phi} \\ & + \frac{1}{2} (\partial_\mu \vec{\phi})^2 + V(\vec{\phi}), \end{aligned} \quad (8)$$

where  $V(\vec{\phi})$  is the meson and diquark potential whose precise form will be specified later. A non-vanishing chemical potential couples not only to the quarks but also to the bosonic diquarks. Rewriting Eq. (8) in terms of the original variables we obtain the quark-meson-diquark (QMD) model Lagrangian

$$\begin{aligned} \mathcal{L}_{\text{QMD}} = & \bar{\psi} (\not{D} + g(\sigma + i\gamma^5 \vec{\pi} \vec{\tau}) - \mu\gamma^0) \psi \\ & + \frac{g}{2} (\Delta^* (\psi^T C \gamma^5 \tau_2 S \psi) + \Delta (\psi^\dagger C \gamma^5 \tau_2 S \psi^*)) \\ & + \frac{1}{2} (\partial_\mu \sigma)^2 + \frac{1}{2} (\partial_\mu \vec{\pi})^2 + V(\vec{\phi}) \\ & + \frac{1}{2} ((\partial_\mu - 2\mu \delta_\mu^0) \Delta) (\partial_\mu + 2\mu \delta_\mu^0) \Delta^*, \end{aligned} \quad (9)$$

with  $C = \gamma^2 \gamma^0$  and a flavor- and color-blind Yukawa coupling  $g$ . With

$$V(\vec{\phi}) = \frac{\lambda}{4} (\vec{\phi}^2 - v^2)^2 - c\sigma, \quad (10)$$

one obtains the corresponding  $O(6)$  linear sigma model; and in the limit  $\lambda \rightarrow \infty$ , the bosonic part of  $\mathcal{L}_{\text{QMD}}$  is equivalent to the leading-order  $\chi\text{PT}$  Lagrangian of Refs. [7]. To see this explicitly it is best to start from the latter, use the explicit coset parametrization of [11] as given above, and make the identifications  $v = f_\pi = 2F$  and  $c = f_\pi m_\pi^2 = 2Fm_\pi^2$ . It maybe worthwhile mentioning that the coefficient of the leading term in  $\mu$  of the  $\chi\text{PT}$  Lagrangian,  $\mu^2 \text{tr}(\Sigma B^T \Sigma^\dagger B)$  with  $B = UB_0U^\dagger$ , which was fixed from gauging the flavor  $SU(4)$  in [6], here simply follows from  $-2\mu^2|\Delta|^2$  as part of the kinetic term of the complex scalar diquark field  $\Delta$  with chemical potential  $\mu_B = 2\mu$ . This implies in particular, that the meson/diquark potential  $V(\vec{\phi})$  itself, up to the explicit breaking by  $-\sigma$ , which needs to be only  $SO(4) \times SO(2)$  invariant in general at finite  $\mu$ , must remain  $SO(6)$  invariant, however, at this leading order,  $\mathcal{O}(\mu^2)$ , and therefore at  $\mathcal{O}(\phi^2)$  in the fields, likewise. We can thus only have an  $SO(6)$  invariant mass term in  $V(\vec{\phi})$ .

In the following it will be more convenient to rewrite the Lagrangian in terms of Nambu-Gorkov-like spinors  $\Psi = \begin{pmatrix} \psi_r \\ \tau_2 \psi_g^c \end{pmatrix}$ , where  $\psi_r$  ( $\psi_g$ ) denote the red (green) color components of  $\psi$  and  $\psi^c \equiv C\bar{\psi}^T$  as in [28]. This yields

$$\begin{aligned} \mathcal{L}_{\text{QMD}} = & \bar{\Psi} S_0^{-1} \Psi + \frac{1}{2}(\partial_\mu \sigma)^2 + \frac{1}{2}(\partial_\mu \vec{\pi})^2 + V(\vec{\phi}) \\ & + \frac{1}{2}((\partial_\mu - 2\mu\delta_\mu^0)\Delta)(\partial_\mu + 2\mu\delta_\mu^0)\Delta^*, \end{aligned} \quad (11)$$

where

$$S_0^{-1} = \begin{pmatrix} \not{\partial} + g(\sigma + i\gamma^5 \vec{\pi} \vec{\tau}) - \gamma^0 \mu & g\gamma^5 \Delta \\ -g\gamma^5 \Delta^* & \not{\partial} + g(\sigma - i\gamma^5 \vec{\pi} \vec{\tau}) + \gamma^0 \mu \end{pmatrix}. \quad (12)$$

Gauge field dynamics and confinement effects can be modeled also in  $\text{QC}_2\text{D}$  by including a constant Polyakov-loop variable as a background field as in the NJL model [28], and analogous to what is commonly done in the so-called Polyakov-loop-extended quark-meson models of three-color QCD [46–48]. To this end one introduces a constant temporal background gauge field  $A_\mu = A_0 \delta_{\mu 0}$  which is furthermore assumed to be in the Cartan subalgebra as in the Polyakov gauge, *i.e.*, for  $SU(2)_c$  simply given by  $A_0 = T^3 2a_0$ . This leads to the Polyakov loop variable

$$\Phi \equiv \frac{1}{2} \text{Tr}_c e^{i\beta A_0} = \cos(\beta a_0), \quad (13)$$

to model a thermal expectation value of the color-traced Polyakov loop at an inverse temperature  $\beta = 1/T$ , as an order parameter for the deconfinement transition at vanishing chemical potential. The covariant derivative  $D_\mu = \partial_\mu - i\delta_{\mu 0} A_0$  leads to an additional contribution of the form  $-i\bar{\psi}\gamma^0 T^3 2a_0 \psi$  which can be rewritten as  $-i\bar{\Psi}\gamma^0 a_0 \Psi$  in terms of the spinor field  $\Psi$ . Finally, we then arrive at the Polyakov-loop-extended quark-meson-diquark model (PQMD) Lagrangian,

$$\mathcal{L}_{\text{PQMD}} = \mathcal{L}_{\text{QMD}} - i\bar{\Psi} \begin{pmatrix} \gamma^0 a_0 & 0 \\ 0 & \gamma^0 a_0 \end{pmatrix} \Psi + \mathcal{U}_{\text{Pol}}(\Phi), \quad (14)$$

with  $\mathcal{L}_{\text{QMD}}$  defined in Eq. (11) and  $\mathcal{U}_{\text{Pol}}(\Phi)$  is the Polyakov-loop potential [28] which is commonly fitted to lattice results, but which can also be computed with functional methods [49, 50]. In contrast to the three-color case the Polyakov-loop potential is a function of one single real variable  $\Phi$  here, even in the presence of a diquark condensate.

### III. MEAN-FIELD THERMODYNAMICS

The grand potential in mean-field approximation is obtained by integrating over the quark fields and neglecting bosonic fluctuations. This means that all mesonic and diquark fields are replaced by their constant expectation values  $\sigma \equiv \langle \sigma \rangle$ ,  $\Delta \equiv \langle \Delta \rangle$ ,  $\Delta^* \equiv \langle \Delta^* \rangle$  and  $\vec{\pi} \equiv \langle \vec{\pi} \rangle = \vec{0}$ . In momentum space we then obtain,

$$\mathcal{L}_{\text{PQMD}}^{\text{MF}} = \bar{\Psi} \left( S_{0,\text{MF}}^{-1} - i\gamma^0 a_0 \right) \Psi + V_{\text{MF}}(\sigma, d^2) + \mathcal{U}_{\text{Pol}}(\Phi), \quad (15)$$

where

$$S_{0,\text{MF}}^{-1} = \begin{pmatrix} -i\not{p} - \gamma^0 \mu + g\sigma & g\gamma^5 \Delta \\ -g\gamma^5 \Delta^* & -i\not{p} + \gamma^0 \mu + g\sigma \end{pmatrix}, \quad (16)$$

and  $V_{\text{MF}}(\sigma, d^2) = (\lambda/4)(\sigma^2 + d^2 - v^2)^2 - c\sigma - 2\mu^2 d^2$  with  $d^2 \equiv |\Delta|^2$  is the bosonic effective potential. The last term comes from the kinetic diquark part of Eq. (11) and is included in the effective potential here. This term and the explicit chiral symmetry breaking by  $-\sigma$  break the  $SU(4)$  symmetry of the effective potential  $V_{\text{MF}}$ . The details of the parameter fixing and the values used in the numerical calculations are given in Appendix A.

The fermion-loop integration then yields for the grand potential  $\Omega$ ,

$$\begin{aligned} \Omega(T, \mu) = & -T \sum_{n \in Z} \int \frac{d^3 p}{(2\pi)^3} \text{Tr} \ln (S_{0,\text{MF}}^{-1} - i\gamma^0 a_0) \\ & + V_{\text{MF}}(\sigma, d^2) + \mathcal{U}_{\text{Pol}}(\Phi), \end{aligned} \quad (17)$$

where the trace runs over internal indices (Dirac-, flavor- and Nambu-Gorkov space) and we sum over antiperiodic Matsubara modes  $\nu_n = (2n + 1)\pi T$ . The four distinct eigenvalues of  $\gamma^0 S_{0,\text{MF}}^{-1}$  are given by  $\pm E_p^\pm - i\nu_n$  and  $\pm E_p^- - i\nu_n$  with

$$\begin{aligned} E_p^\pm &= \sqrt{g^2 d^2 + \epsilon_p^{\pm 2}}, \\ \epsilon_p^\pm &= \epsilon_p \pm \mu \quad \text{and} \quad \epsilon_p = \sqrt{\vec{p}^2 + g^2 \sigma^2}. \end{aligned} \quad (18)$$

The Matsubara sum can be performed analytically with the result

$$\begin{aligned} \Omega(\sigma, d^2, \Phi) = & -4 \int \frac{d^3 p}{(2\pi)^3} \left\{ E_p^+ + E_p^- \right. \\ & + T \ln \left( 1 + 2\Phi e^{-\beta E_p^+} + e^{-2\beta E_p^+} \right) \\ & + T \ln \left( 1 + 2\Phi e^{-\beta E_p^-} + e^{-2\beta E_p^-} \right) \left. \right\} \\ & + V_{\text{MF}}(\sigma, d^2) + \mathcal{U}_{\text{Pol}}(\Phi). \end{aligned} \quad (19)$$

When the bosonic potential  $V_{\text{MF}}$  is replaced by  $M^2(\sigma^2 + d^2) - c\sigma$ , with  $M^2 = g^2/(4G)$  and  $c = 2gm_0/(4G)$ , this coincides with the Hubbard-Stratonovich transformed PNJL model result [28] with four-quark coupling  $G$  and current-mass parameter  $m_0$ . Note that the model independent  $-2\mu^2 d^2$  term from chiral effective field theory, which is included in the bosonic part of the (P)QMD model, does not explicitly show up in the grand potential of the (P)NJL model. Minimizing the thermodynamic potential with respect to the constant mean fields  $\sigma, d, \Phi$  leads to the gap equations,

$$\frac{\partial\Omega}{\partial\sigma} = \frac{\partial\Omega}{\partial d} = \frac{\partial\Omega}{\partial\Phi} = 0, \quad (20)$$

whose simultaneous solution yields the temperature and chemical potential dependent condensates  $\sigma, d$  and  $\Phi$ .

### A. Vacuum contributions

The fermion-loop contribution to the grand potential in mean-field approximation, Eq. (19), contains an ultraviolet divergent vacuum part. In the standard *no-sea* mean-field approximation one usually dismisses this vacuum contribution to the bulk thermodynamics. For some phenomenological consequences of this additional approximation and its influence on mean-field results, see Ref. [51, 52] and the references therein. Here we add an observation concerning this mean-field ambiguity of the quark-meson model when viewed as the  $d \rightarrow 0$  limit of the quark-meson-diquark model grand potential. Because the Polyakov-loop contributions are irrelevant here we set  $\Phi = 1$ .

For  $d = 0$  Eq. (19) superficially appears to reduce to the conventional mean-field expression for the grand potential of the quark-meson model [53] up to an overall  $N_c$  in front of the fermion-loop contribution  $\Omega_q$ ,

$$\Omega_q = \Omega_q^{\text{vac}} - 4N_c T \int \frac{d^3p}{(2\pi)^3} \sum_{\pm} \ln \left( 1 + e^{-\beta(\epsilon_p \pm \mu)} \right). \quad (21)$$

We illustrate the effect of the vacuum contribution for  $N_c = 2$  colors but without diquark condensate (*i.e.* with  $d = 0$ ) in Fig. 2. To regularize the vacuum term  $\Omega_q^{\text{vac}}$  we employ a simple three-momentum cutoff  $\Lambda$  and assess the dependence of the phase structure on  $\Lambda$ . The parameters are fixed to reproduce an  $\sqrt{N_c}$ -scaled  $f_\pi = 76$  MeV and a pion screening mass of  $m_\pi = 138$  MeV. In each case the sigma meson mass is adjusted so as to yield a common value for a chiral transition at  $\mu = 0$  of  $T_c \approx 183$  MeV.  $\Lambda = 0$  corresponds to the no-sea approximation. The dependence of the position of the critical endpoint (CEP) at  $\mu_c$  on the cutoff  $\Lambda$  is clearly visible in Fig. 2. With increasing  $\Lambda$  its location gets shifted towards larger chemical potentials and approaches the dimensionally regularized result [51] when  $\Lambda/\mu_c$  is sufficiently large.

More carefully, however, one observes that the fermion-loop in the no-sea approximation ( $\Omega_q^{\text{vac}} = 0$  when  $\Lambda = 0$ )

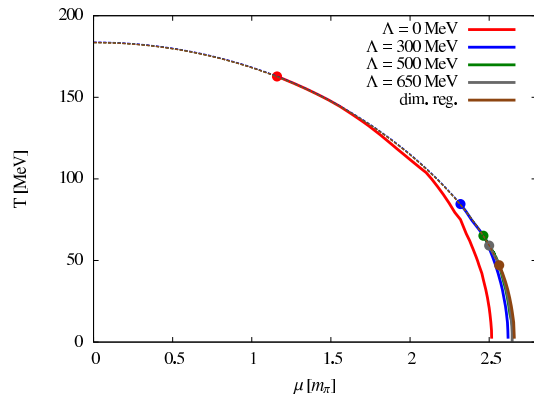


FIG. 2. Standard  $N_c = 2$  QM phase diagram: dependence of the location of the CEP on the vacuum-term cutoff  $\Lambda$  in comparison to dimensional regularization.

in Eq. (21) does not tend to zero for  $T \rightarrow 0$  when  $\mu > g\sigma$ , but still contains temperature independent contributions from momenta with  $\vec{p}^2 < \mu^2 - g^2\sigma^2$ .

On the other hand, the  $d \rightarrow 0$  limit of Eq. (19) with

$$E_p^- \rightarrow |\epsilon_p - \mu| \quad (22)$$

yields a grand potential of the quark-meson model for two colors which depends only on the chiral condensate  $\sigma$  but which differs from the conventional expression by the appearance of the modulus of the quasi-particle energies,

$$\begin{aligned} \Omega(\sigma) = & -4 \int \frac{d^3p}{(2\pi)^3} \left\{ \epsilon_p + \mu + |\epsilon_p - \mu| \right. \\ & + 2T \ln \left( 1 + e^{-\beta(\epsilon_p + \mu)} \right) \\ & \left. + 2T \ln \left( 1 + e^{-\beta|\epsilon_p - \mu|} \right) \right\} + V_{\text{MF}}(\sigma, 0). \end{aligned} \quad (23)$$

The last two terms herein deserve to be called thermal now, as they do vanish at zero temperature for all  $\mu$ . When vacuum and the thermal contributions are regularized in the same way we can recover the usual expression by means of the identity

$$|x| + 2 \ln(1 + \exp(-|x|)) = 2 \ln \cosh(x/2) + 2 \ln 2. \quad (24)$$

This is for example the case in the NJL model if one chooses to regulate both thermal and vacuum parts with a three-momentum cutoff, but this is not what is usually done in the quark-meson model where the ultraviolet finite thermal contributions are meant to be fully retained. The cutoff in the phase diagrams of Fig. 2 was applied only to  $\Omega_q^{\text{vac}}$  in Eq. (21), likewise. Otherwise the picture would change yet again. This is a bit of a grain of salt for the no-sea mean-field approximation in quark-meson models which is best motivated phenomenologically as modelling the restoration of chiral symmetry at  $T = 0$  for large chemical potentials. Luckily, the problem is irrelevant altogether, once fluctuations are included via the functional renormalization group for which the quark-meson model shows its true uses.

Meanwhile, for the mean-field analysis of our quark-meson-diquark model including the possibility of diquark condensation with  $d \neq 0$ , we really have no option other than the perhaps anyway more natural splitting of thermal and vacuum contributions based on the modulus of the quasi-particle energy as the  $d \rightarrow 0$  limit of  $E_p^-$  in the QMD model mean-field grand potential, Eq. (19).

If one considers the difference between cutting off the vacuum term in Eq. (21) as compared to the one in Eq. (23) as measure for the reliability of the calculation, one is led to conclude that the cutoff  $\Lambda$  in  $\Omega_q^{\text{vac}}$  should always be larger than the chemical potential  $\mu$ .

In the following we will continue to regulate vacuum terms with a sharp momentum cutoff mainly because dimensional regularization, as applied to the three-color PQM model in [51], due to the structure of  $E_p^\pm$ , gets too complicated for a semi-analytic treatment here, with full diquark mean fields from the grand potential in Eq. (19).

## B. Diquark condensation

Independent of the discussion in the previous section and of the influence of fluctuations, we know for two-color QCD that the quark-meson-model-like phase diagrams of the form as those in Fig. 2 are wrong. The exact chiral effective field theory results [6, 7] from the symmetries and breaking patterns as reviewed in Sec. II A tell us that we must include the diquark condensate along with the chiral condensate and base our mean-field analysis on Eqs. (19), (20) in order to describe the superfluid diquark phase starting at a critical line  $\mu_c(T)$  with  $\mu_c(0) = m_\pi/2$  (or  $\mu_B = m_B$ ).

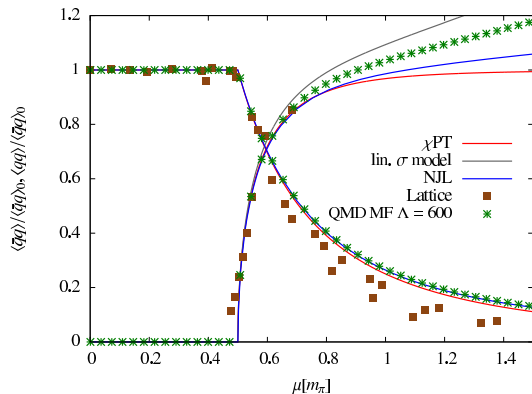


FIG. 3. Condensates at  $T = 0$  (NJL parameter values from [26]; lattice data from [17]; linear sigma model with  $m_\pi = 138$  MeV and  $m_\sigma = 680$  MeV).

The resulting chemical potential dependence of the chiral and diquark condensates at zero temperature is shown in Fig. 3 where we compare the prediction from leading order chiral perturbation theory [7], the NJL [26] and the linear sigma model [29] results with lattice data [17] and

our quark-meson-diquark model mean-field result with vacuum contribution from Eqs. (19), (20).

The  $T = 0$  onset of diquark condensation at  $\mu_c(0) = m_\pi/2$  as an exact result is built-in in  $\chi$ PT and the  $O(6)$  linear sigma model as discussed in Sec. II B. Therefore, it also holds for the screening mass of the pion from the bosonic potential in our adapted no-sea approximation, which reduces to the linear sigma model at  $T = 0$  by definition. They both go beyond the leading order chiral perturbation theory in that they include effects of a finite sigma meson mass. The linear sigma model expressions for the  $T = 0$  condensates are [29]

$$\frac{\sigma}{\sigma_0} = \begin{cases} 1 & \text{for } \mu < \mu_c \\ \frac{1}{x^2} & \text{for } \mu > \mu_c \end{cases} \quad (25)$$

$$\frac{|\Delta|}{\sigma_0} = \begin{cases} 0 & \text{for } \mu < \mu_c \\ \sqrt{1 - \frac{1}{x^4} + 2\frac{x^2-1}{y^2-1}} & \text{for } \mu > \mu_c \end{cases},$$

where  $x = 2\mu/m_\pi$  and  $y = m_\sigma/m_\pi$ . The only difference between these and the  $\chi$ PT result [7] is the  $y$ -dependent term in the diquark condensate which reduces to the  $\chi$ PT formula for  $y \rightarrow \infty$ . Note that the chiral condensate does not depend on the sigma meson mass whereas the diquark condensate does via  $y$  which explains the variations of the diquark condensates at large  $\mu$  in Fig. 3.

Beyond the no-sea approximation, one needs to distinguish between screening and pole mass. Only the latter agrees with the onset baryon chemical potential at the mean-field level, in general. We will discuss this in more detail in the next subsection.

The overall agreement of our  $T = 0$  results with the existing literature in Fig. 3 is very reassuring. In particular, there is no dependence on the chemical potential for  $\mu < \mu_c$  in accordance with the Silver Blaze property as also discussed more in Sec. III C below.

Common to all studies, the chiral condensate decreases with increasing  $\mu$  in the diquark condensation phase above  $\mu_c$ . As a result, the quark-meson-model-like 1<sup>st</sup> order transition line and CEP at  $\mu$  around  $2.5m_\pi$  are completely gone, as seen also in Fig. 4.

Fig. 4 shows the phase diagram of two QMD model mean-field calculations in comparison with the result of an NJL model recalculation following Ref. [26]. For small chemical potentials and small temperatures one finds the chirally broken phase with vanishing diquark condensate crossing over with increasing temperature to the phase with asymptotically restored chiral symmetry as usual. In addition, there is the diquark condensation phase for  $\mu > \mu_c(T)$  characterized by non-zero baryon density.

The NJL model calculations show a continuous diquark condensation transition throughout the whole phase diagram [28]. In contrast, in our mean-field QMD model results here, the second order line  $\mu_c(T)$  ends in a tricritical point from where on towards larger chemical potentials it becomes a 1<sup>st</sup> order transition. Such a behavior was also predicted at next-to-leading order  $\chi$ PT [9], where it was concluded that this tricritical point occurred at  $\mu_c \approx 0.57m_\pi$  and  $T \approx 220$  MeV. The temperature

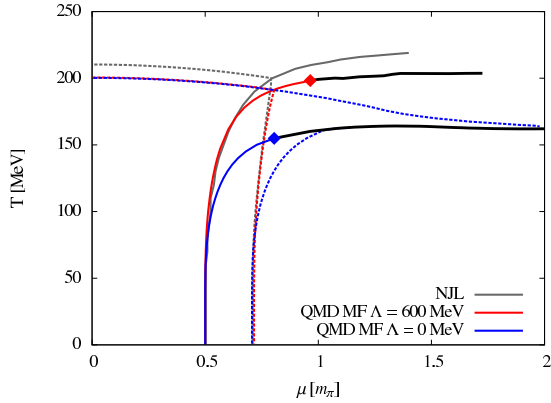


FIG. 4. Mean field phase diagrams: QMD model (with and without vacuum term) vs. NJL model (with parameters from [26]); dashed: chiral crossover; solid: second order transition; thick solid black: first order transition; diamonds: tricritical points as predicted in [9].

range is quite comparable here, but its precise location depends on the value for the vacuum-term cutoff  $\Lambda$  and moves towards larger chemical potentials with increasing  $\Lambda$ . Moreover, as we will see below, the first-order transition will be washed out by fluctuations which will make it second-order again, and it is hence a mean-field artifact.

$$\Gamma_{\text{tl}}^{(2)}(p) = \begin{pmatrix} p^2 - m^2 + \lambda\phi^2 + 2\lambda\sigma^2 & 2\lambda\sigma d & 0 \\ 2\lambda\sigma d & p^2 - 4\mu^2 - m^2 + \lambda\phi^2 + 2\lambda d^2 & -4\mu p_0 \\ 0 & 4\mu p_0 & p^2 - 4\mu^2 - m^2 + \lambda\phi^2 \end{pmatrix}. \quad (28)$$

The RPA polarization functions are obtained from evaluating the fermion-loop integrals with external momentum  $p$  in the usual way,

$$\Pi_{ij}(p) = \text{Tr}_q \left[ \frac{\partial \Gamma_F^{(2)}}{\partial \phi_i} \Big|_{\phi_{\text{MF}}} G_{\text{MF}}(p+q) \frac{\partial \Gamma_F^{(2)}}{\partial \phi_j} \Big|_{\phi_{\text{MF}}} G_{\text{MF}}(q) \right], \quad (29)$$

where  $G_{\text{MF}} = (\Gamma_F^{(2)}|_{\phi_{\text{MF}}})^{-1}$ . They can be found in the NJL model literature [28, 39, 40], originally from the two-flavor three-color standard NJL model with isospin chemical potential and pion condensation. Since the available expressions are either incomplete or at variance with our computations, we have recomputed them and list the complete explicit expressions for these polarization functions as a convenience to the reader in Appendix C.

To find the pole masses we use  $p = (-i\omega, \vec{0})$  and the somewhat sloppy notations  $\Gamma^{(2)}(\omega) \equiv \Gamma^{(2)}(p = (-i\omega, \vec{0}))$ ,

### C. Pole versus screening masses

The definition of meson/diquark masses is absolutely crucial already at mean-field level to get results which are consistent with the Silver Blaze property. As soon as one goes beyond the no sea approximation there is an important distinction between the screening mass at zero external momentum, which is just determined by the curvature of the effective potential, and the pole mass which takes into account a non-vanishing external momentum. The latter is the natural choice in NJL model calculations but has so far not been taken into account in QM model studies. Both definitions coincide for massless particles and in the no sea approximation.

The meson/diquark pole masses are defined as the zeroes of the determinant of their inverse propagator,

$$\Gamma_{ij}^{(2)}(p) = \Gamma_{\text{tl}}^{(2)}(p)_{ij} + \Pi_{ij}(p), \quad (26)$$

where, for the pions,

$$\Gamma_{\text{tl}}^{(2)}(p)_{ij} = (p^2 - m^2 + \lambda\phi^2)\delta_{ij}, \quad i, j = 2, 3, 4, \quad (27)$$

with  $m^2 = \lambda v^2$  from the tree-level potential (10) and  $\phi^2 = \sigma^2 + d^2$ . When the diquark condensate  $d$  is non-zero, we choose it to lie in the  $\phi_5 = \text{Re } \Delta$  direction without loss, the sigma meson mixes with the scalar diquark pair already at tree-level through the  $O(6)$  linear sigma model potential (10). In the 3-dimensional subspace of sigma and diquarks in the real basis  $\phi_5 = \text{Re } \Delta$ ,  $\phi_6 = \text{Im } \Delta$ ,

$\Pi(\omega) \equiv \Pi(p = (-i\omega, \vec{0}))$ , to solve

$$\det \Gamma^{(2)}(\omega) = 0, \quad \text{for } \omega = m_k, \quad k = 1, \dots, 6. \quad (30)$$

The polarization integrals are ultraviolet divergent. As before, we use a spatial momentum cutoff  $\Lambda$  for the temperature-independent contributions. Making the  $T$ -dependence explicit, we may thus write,

$$\begin{aligned} \Pi^{\text{reg}}(\omega, T) &= \Pi^{\text{th}}(\omega, T) + \Pi_{\Lambda}^{\text{vac}}(\omega), \quad \text{where} \\ \Pi^{\text{th}}(\omega, T) &= \Pi(\omega, T) - \Pi(\omega, 0) \end{aligned} \quad (31)$$

is ultraviolet finite. In the normal phase with  $d = 0$ , *i.e.*, for  $\mu$  below the onset of diquark condensation at  $\mu_c(T)$ , the polarization integrals are diagonal in the basis where  $\Delta = \phi_5 + i\phi_6$  and  $\Delta^* = \phi_5 - i\phi_6$ . The polarization matrix

$\Pi(\omega, T)$  from App. C is then diagonal with entries [28],

$$\begin{aligned}\Pi_\sigma(\omega, T) &= 16N_c g^2 \int \frac{d^3 q}{(2\pi)^3} \frac{\bar{q}^2}{\epsilon_q} \frac{1 - N_q(\epsilon_q^-) - N_q(\epsilon_q^+)}{\omega^2 - 4\epsilon_q^2} \\ &\quad + 4N_c g^2 \delta_{\omega,0} \int \frac{d^3 q}{(2\pi)^3} \frac{g^2 \sigma^2}{\epsilon_q^2} (N'_q(\epsilon_q^+) + N'_q(\epsilon_q^-)) \\ \Pi_\pi(\omega, T) &= 16N_c g^2 \int \frac{d^3 q}{(2\pi)^3} \frac{\epsilon_q (1 - N_q(\epsilon_q^-) - N_q(\epsilon_q^+))}{\omega^2 - 4\epsilon_q^2} \\ \Pi_\pm(\omega, T) &= 4N_c g^2 \int \frac{d^3 q}{(2\pi)^3} \left( \frac{1 - 2N_q(\epsilon_q^\mp)}{\omega - 2\epsilon_q^\mp} - \frac{1 - 2N_q(\epsilon_q^\pm)}{\omega + 2\epsilon_q^\pm} \right)\end{aligned}\quad (32)$$

with  $\epsilon_q^\pm = \sqrt{\bar{q}^2 + g^2 \sigma^2} \pm \mu$ ,  $\Pi_\pm$  for  $\Delta$ ,  $\Delta^*$  and Polyakov loop enhanced quark/antiquark occupation numbers

$$N_q(E) \equiv N_q(E; T, \Phi) = \frac{1 + \Phi e^{\frac{E}{T}}}{1 + 2\Phi e^{\frac{E}{T}} + e^{\frac{2E}{T}}}, \quad (33)$$

which simplify to the Fermi-Dirac distribution for  $\Phi = 1$ .

As usual, these expressions are obtained from analytically continuing the results for imaginary discrete values  $\omega = i2\pi T n$  corresponding to the Matsubara frequencies in imaginary time. To make the continuation unique, one usually assumes in addition that the polarization functions are well behaved at complex infinity with cuts only along the real axis. Then, it follows that the correspondingly continued expressions for finite spatial momenta,  $\Pi(p = (-i\omega, \vec{p}))$  are non-analytic at the origin in momentum space, with different limits for  $\omega \rightarrow 0$  at  $\vec{p} = 0$  or for  $|\vec{p}| \rightarrow 0$  at  $\omega = 0$ . The first limit yields a plasmon mass, associated with the damping of plasma oscillations, while the second is the one that yields the correct finite temperature screening masses [54]. Here, in the normal phase the two differ only for the sigma meson, by the  $n = 0$  contribution proportional to  $\delta_{\omega,0}$  in the equation for  $\Pi_\sigma(\omega, T)$ , which can be obtained from the expression for  $\Pi_\sigma(p = (-i\omega, \vec{p}))$  in Ref. [28] with the additional prescription to set  $\omega = 0$  first and then take  $|\vec{p}| \rightarrow 0$ .

The corresponding extra contributions for  $\omega = 0$  in the diquark condensation phase are also given in App. C. None of them are really needed here. In particular, the  $\delta_{\omega,0} \Pi^0(T)$  contributions vanish for  $T \rightarrow 0$ , but they assure that the screening masses extracted from the propagators agree with the corresponding ones from the effective potential also at finite temperature, see below.

Setting  $\Phi = 1$  and dismissing the temperature dependent contributions  $\delta_{\omega,0} \Pi^0(T)$ , the polarization functions agree with the ones from Ref. [39, 40] for baryon chemical potential  $\mu_B = 0$  and isospin chemical potential  $\mu_I = 2\mu$ , where  $\Pi_\pi$  and  $\Pi_\pm$  belong to neutral and charged pions, respectively.

The RPA pole masses in the quark-meson-diquark model in the normal phase are then simply given by the

solutions of the following equations,

$$\begin{aligned}m_\sigma : \quad & \omega^2 = -m^2 + 3\lambda\sigma^2 + \Pi_\sigma(\omega, T) \\ m_\pi : \quad & \omega^2 = -m^2 + \lambda\sigma^2 + \Pi_\pi(\omega, T) \\ m_\pm : \quad & (\omega \pm 2\mu)^2 = -m^2 + \lambda\sigma^2 + \Pi_\pm(\omega, T)\end{aligned}\quad (34)$$

If we use the mean-field expression in Eq. (19) for the fermionic pressure with chiral and diquark condensates in the form,

$$\Omega_q(T, \mu) = -4T \int \frac{d^3 q}{(2\pi)^3} \sum_\pm \ln \left( 2 \left( \cosh \left( \frac{E_q^\pm}{T} \right) + \Phi \right) \right), \quad (35)$$

one immediately verifies that the polarization functions for external momentum  $p = 0$ , corresponding to the limit  $|\vec{p}| \rightarrow 0$  at  $\omega = 0$  in the imaginary time formalism,

$$\begin{aligned}\Pi_\sigma(0, T) &= 2 \frac{\partial}{\partial \sigma^2} \Omega_q(T, \mu) \Big|_{d=0} + 4\sigma^2 \frac{\partial^2}{\partial (\sigma^2)^2} \Omega_q(T, \mu) \Big|_{d=0}, \\ \Pi_\pi(0, T) &= 2 \frac{\partial}{\partial \sigma^2} \Omega_q(T, \mu) \Big|_{d=0}, \\ \Pi_\pm(0, T) &= \Pi_\pm(0, T) = 2 \frac{\partial}{\partial d^2} \Omega_q(T, \mu) \Big|_{d=0}.\end{aligned}\quad (36)$$

This shows explicitly that the screening masses, defined by these derivatives of the effective potential, are obtained as the constant contributions in Eqs. (34) for  $\omega = 0$ ,

$$\begin{aligned}m_\sigma^{\text{sc}2} &= -m^2 + 3\lambda\sigma^2 + \Pi_\sigma(0, T), \\ m_\pi^{\text{sc}2} &= -m^2 + \lambda\sigma^2 + \Pi_\pi(0, T), \\ m_\pm^{\text{sc}2} &= -4\mu^2 - m^2 + \lambda\sigma^2 + \Pi_\pm(0, T).\end{aligned}\quad (37)$$

This is true at all temperatures in the normal phase. Note also that because  $\Pi_+(0, T) = \Pi_-(0, T)$ , the baryon chemical potential  $\mu_B = 2\mu$  never splits the diquark and antiquark screening masses,  $m_+^{\text{sc}}(T, \mu) = m_-^{\text{sc}}(T, \mu)$ .

At any temperature we furthermore verify for  $\mu = 0$  that  $\Pi_\pi(\omega, T) = \Pi_\pm(\omega, T)$ , *i.e.*, pion and diquark masses are degenerate as they must from  $SO(5)$  symmetry. Moreover, the gap equation for the chiral condensate reduces in the chiral limit  $c \rightarrow 0$  to the condition for massless pions, as usual, and both these observations hold for screening and pole masses, likewise.

Finally, but maybe most importantly, the gap equation for the diquark condensate reads

$$\frac{\partial}{\partial d} \Omega = d \left( -m^2 + \lambda\sigma^2 - 4\mu^2 + 2 \frac{\partial}{\partial d^2} \Omega_q(T, \mu) \right) \stackrel{!}{=} 0, \quad (38)$$

and the critical line  $\mu_c(T)$  is defined by the condition that the terms in brackets vanish for  $d = 0$  so that a second zero develops there. This is equivalent to the diquark pole masses being  $m_- = 0$  and  $m_+ = 4\mu$ . While their screening masses  $m_\pm^{\text{sc}}$  both vanish at  $\mu = \mu_c$ , for the pion and diquark pole masses we have the general exact zero-temperature relation

$$\Pi_\pm(\omega, 0) = \Pi_\pi(\omega \pm 2\mu, 0) \Rightarrow m_\pm = m_\pi \pm 2\mu, \quad (39)$$

in the normal phase where  $m_\pi = m_{\pi,0}$  remains independent of  $\mu$  until  $2\mu = m_{\pi,0}$  as required by the Silver Blaze property.

In contrast, the same relation entails for the degenerate diquark screening masses ( $\Pi_\pi$  is an even function of  $\omega$ ),

$$m_\pm^{\text{sc}2} = m_\pi^{\text{sc}2} - 4\mu^2 + \Pi_\pi(2\mu, 0) - \Pi_\pi(0, 0), \quad (40)$$

which reiterates that diquark and pion screening masses are also degenerate at  $\mu = 0$ , but that both diquark screening masses  $m_\pm^{\text{sc}}$  vanish as  $2\mu$  approaches the ( $\mu$ -independent) pion pole mass  $m_\pi$  from below.

The bottom line is that the onset of diquark condensation at  $\mu_B = 2\mu = 2\mu_c(0)$ , whatever the screening mass may be, *defines* the physical zero-temperature pion mass. We will make use of this property to fix the pion mass in the RG calculation, where the calculation of the pole mass is more involved.

In the diquark-condensation phase the sigma meson mixes with the two diquark modes, *i.e.*, the respective masses have to be determined from the zeroes of the determinant of the corresponding  $3 \times 3$  submatrix in  $\Gamma^{(2)}(\omega)$ . As in the NJL model [28, 39] one can verify further exact results from the mass formulas at  $T = 0$ . Also in the QMD model at mean-field/RPA level the in-medium pion pole-mass is equal to  $m_\pi = 2\mu$  above the onset of diquark condensation at  $2\mu = m_{\pi,0}$ . Moreover, one verifies explicitly that one of the three modes in the diquark/sigma sector remains exactly massless in the superfluid phase, also at finite temperature. This is of course the Goldstone boson corresponding to the spontaneously broken  $U(1)_B$  baryon number. Another one becomes degenerate with the pions for large values of the chemical potential, eventually, reflecting the restoration of chiral symmetry. They combine into an  $SO(4)$  multiplet as the chiral condensate vanishes for large chemical potentials.

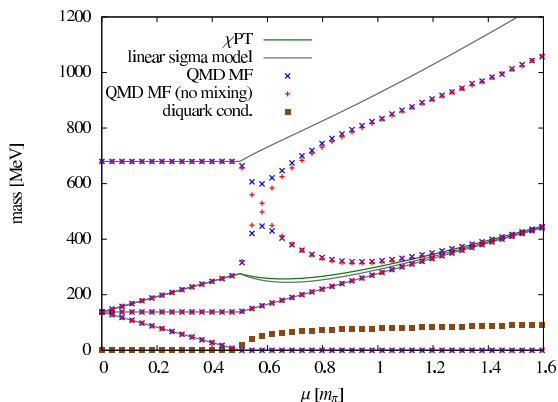


FIG. 5. Pole-mass spectrum at  $T = 0$ : mean-field/RPA QMD model results (with vacuum-term cutoff  $\Lambda = 600$  MeV), for comparison also shown without the effect of diquark/sigma-meson mixing in the superfluid phase, vs. linear sigma model.

This is all nicely reflected in the numerical results shown in Fig. 5. As the RPA pole-mass formulas imply, the meson masses stay constant in the normal phase whereas the diquark masses are split up from the constant  $m_B = m_\pi$  by the terms  $\pm\mu_B$  due to their coupling to the baryon chemical potential  $\mu_B = 2\mu$ .

The diquark and sigma masses in the phase of diquark condensation show a considerable dependence on the inclusion of the vacuum term. This can be seen, for example, by comparing the QMD model results with vacuum-term cutoff  $\Lambda = 600$  MeV to those from the linear sigma model, which are identical to the ones in the no-sea approximation ( $\Lambda = 0$ ). In the linear sigma model, the pole masses can simply be calculated from the curvature of the potential. In the normal phase they are simply given by the expected constant  $m_\pi = m_{\pi,0}$ ,  $m_\sigma = m_{\sigma,0}$ , and  $m_\pm = m_{\pi,0} \pm 2\mu$ . In the phase with diquark condensation ( $\mu > \mu_c$ ), on the other hand, we obtain for the linear-sigma model masses,

$$\begin{aligned} m_\pi &= 2\mu \quad m_{\Delta_1} = 0 \\ m_{\sigma/\Delta_2} &= \frac{m_{\pi,0}}{\sqrt{2}} \left( -3 + y^2 + 28x^2 \pm (3(1-y^2)/x^2 \right. \\ &\quad \left. + (-3 + y^2)^2 + 40(-3 + y^2)x^2 + 400x^4)^{\frac{1}{2}} \right)^{\frac{1}{2}}. \end{aligned} \quad (41)$$

with  $x = 2\mu/m_\pi$  and  $y = m_\sigma/m_\pi$  as in Eq. (25).

In addition, Fig. 5 also shows results of a mass calculation where the mixing terms in the sigma/diquark sector were neglected. In those results we have explicitly set the off-diagonal tree-level mixing term  $2\lambda\sigma d$  in Eq. (28) to zero, and used  $\Pi_{\sigma\Delta} = \Pi_{\sigma\Delta^*} = 0$  for the polarization functions of App. C in the superfluid phase. As illustrated in Fig. 5, while the pole masses in the no-sea-approximation are very close to the  $\chi$ PT result, the only difference is due to the finite sigma mass in Eq. (41), the more realistic ones with sufficiently large vacuum-term cutoff are closer to those without any mixing in the crossover region at intermediate chemical potentials.

#### IV. FRG FLOW EQUATIONS

Quantum and thermal fluctuations are of utmost importance in particular near phase transitions and are conveniently included within the framework of the functional renormalization group (FRG) [55–61]. In this work we employ a Wilsonian RG version and investigate the flow equation for the effective average action pioneered by Wetterich [62]. The central object in this approach is the renormalization scale  $k$  dependent effective average action  $\Gamma_k[\Phi]$ , where  $\Phi$  generically represents the set of all quantum fields of the theory. The effective average action interpolates between the microscopic classical action at some ultraviolet (UV) cutoff scale  $k = \Lambda$ , at which fluctuations of essentially all momentum modes are suppressed, and the effective action of the full quantum theory in the

infrared (IR), for  $k \rightarrow 0$ , which then includes all quantum and thermal fluctuations. The scale-dependence is described by the Wetterich flow equation,

$$\partial_t \Gamma_k \equiv k \partial_k \Gamma_k[\Phi] = \frac{1}{2} \text{Tr} \left\{ \partial_t R_k (\Gamma_k^{(2)} + R_k)^{-1} \right\}, \quad (42)$$

which involves a momentum- and scale-dependent regulator  $R_k$ , whose precise form is not fixed but leaves a considerable flexibility. The role of the regulator  $R_k$  is to suppress the fluctuations of modes with momenta below the renormalization scale  $k$ , and the flow equation is UV as well as IR finite.  $\Gamma_k^{(2)}[\Phi]$  are the second functional derivatives of the effective average action with respect to all the fields at scale  $k$ . The functional trace represents a one-loop integration typically evaluated in momentum space and includes the sum over all fields and their internal and space-time indices as well, with standard modifications for fermionic fields. It contains the full field and  $k$ -dependent propagators of the regulated theory with cutoff  $R_k$ , the inverse of  $\Gamma_k^{(2)}[\Phi] + R_k$ . In order to solve the flow equation an initial microscopic action  $S = \Gamma_{k=\Lambda}$  at some UV scale  $\Lambda$  has to be specified. Truncating the effective action to a specific form, the functional equation can be converted into a closed set of (integro-)differential equations, but will in general also introduce some regulator dependence in the flow. The choice of an optimized regulator minimizes this regulator dependence for physical observables. As bosonic (fermionic) regulators  $R_{k,B}$  ( $R_{k,F}$ ) we choose

$$\begin{aligned} R_{k,B}(\vec{p}) &= (k^2 - \vec{p}^2) \theta(k^2 - \vec{p}^2), \\ R_{k,F}(\vec{p}) &= -i\vec{p} \cdot \vec{\gamma} \left( \sqrt{\frac{k^2}{\vec{p}^2}} - 1 \right) \theta(k^2 - \vec{p}^2), \end{aligned} \quad (43)$$

which are three-momentum analogues of the optimized Litim regulators [63]. With this choice the three-

momentum integration becomes trivial and the remaining Matsubara sums can be evaluated analytically. Furthermore, this choice leaves the semilocal  $U(1)$ -symmetry of the Lagrangian unaffected, analogous to [34], where the chemical potential acts like the zero-component of an Abelian gauge field. In addition, these regulators have their precise counterparts in specific three-momentum regulators for proper-time flows which then lead to identical flow equations, c.f. Appendix B. On the other hand, especially in a relativistic system the fact that the zero-component of the momentum is not regulated can potentially be problematic.

Our ansatz for the effective average action in leading-order derivative expansion, where all wave-function renormalization factors are neglected and only the scale-dependent effective potential  $U_k$  is taken into account, reads

$$\Gamma_k = \int d^4x \mathcal{L}_{\text{PQMD}} \Big|_{V+c\sigma \rightarrow U_k}. \quad (44)$$

This means that we use  $\mathcal{L}_{\text{PQMD}}$  from Eq. (14), but replace the meson/diquark potential  $V(\vec{\phi})$  of the  $O(6)$  linear sigma model from Eq. (10) therein by  $U_k - c\sigma$ . The explicit symmetry breaking term  $-c\sigma$  does not affect the flow and is thus not part of  $U_k$  but added after the RG evolution to the full effective potential again. At  $\mu = 0$ , the scale-dependent  $U_k$  then only depends on the modulus of  $\vec{\phi} = (\sigma, \vec{\pi}, \text{Re } \Delta, \text{Im } \Delta)^T$ . At non-vanishing chemical potential, however, we only have  $SO(4) \times SO(2)$  symmetry and must therefore allow it to depend on two invariants, *i.e.*,  $U_k \equiv U_k(\rho^2, d^2)$  where  $\rho^2 = \sigma^2 + \vec{\pi}^2$ , and  $d^2 = |\Delta|^2$  as before. For  $\mu \rightarrow 0$  we recover  $SO(6)$  invariance, of course, so that  $U_k$  then depends only on the combination  $\phi^2 = \rho^2 + d^2$  again.

With the constant field configurations  $\sigma = \rho$ ,  $\vec{\pi} = \vec{0}$ ,  $\text{Re } \Delta = d$ ,  $\text{Im } \Delta = 0$  we obtain for the bosonic second functional derivative of the effective action

$$\Gamma_{k,B}^{(2)} = \begin{pmatrix} p^2 + 2U_{k,\rho} & 0 & 0 & 0 & 0 & 0 & 0 \\ 0 & p^2 + 2U_{k,\rho} & 0 & 0 & 0 & 0 & 0 \\ 0 & 0 & p^2 + 2U_{k,\rho} & 0 & 0 & 0 & 0 \\ 0 & 0 & 0 & p^2 + 2U_{k,\rho} + 4\rho^2 U_{k,\rho\rho} & 4\rho d U_{k,\rho d} & 0 & 0 \\ 0 & 0 & 0 & 4\rho d U_{k,\rho d} & p^2 + 2U_{k,d} + 4d^2 U_{k,dd} - 4\mu^2 & -4\mu p_0 & 0 \\ 0 & 0 & 0 & 0 & 4\mu p_0 & p^2 + 2U_{k,d} - 4\mu^2 & 0 \end{pmatrix}, \quad (45)$$

where we have introduced short-hand notations for the derivatives of the potential with respect to the fields defined as  $U_{k,d} \equiv \partial U_k / \partial d^2$ ,  $U_{k,\rho} \equiv \partial U_k / \partial \rho^2$  and later we will also use  $U_{k,\phi} \equiv \partial U_k / \partial \phi^2$ . Higher order derivatives are labeled with higher order indices accordingly, e.g.,  $U_{k,\rho d} \equiv \partial^2 U_k / \partial \rho^2 \partial d^2$ . The alert reader will have noticed that Eq. (45) agrees with Eqs. (27) and (28) upon working out these derivatives, if we replace  $U_k$  back to

$\lambda(\phi^2 - v^2)^2/4$  which is what we use at  $k = \Lambda$ .

In the fermionic sector we find analogously,

$$\Gamma_{k,F}^{(2)} = \begin{pmatrix} -i\vec{p} - ia_0 \gamma^0 + g\rho - \gamma^0 \mu & g\gamma^5 d \\ -g\gamma^5 d & -i\vec{p} - ia_0 \gamma^0 + g\rho + \gamma^0 \mu \end{pmatrix} \otimes \mathbb{1}_{2 \times 2}. \quad (46)$$

To these expressions we add the respective regulators in Eq. (43) before they are being inverted and inserted into the Wetterich equation Eq. (42), in order to ob-

tain the flow equation for the effective potential. Replacing the zero-components  $p_0$  of the momenta by periodic (antiperiodic) Matsubara frequencies  $\omega_n = 2\pi nT$  ( $\nu_n = (2n + 1)\pi T$ ), and upon performing the spatial

momentum integrations, the corresponding bosonic and fermionic contributions to the flow for the effective potential are then given by the following Matsubara sums,

$$\partial_t U_{k,B} = \frac{k^5 T}{6\pi^2} \sum_{n \in \mathbb{Z}} \left( \frac{3}{\omega_n^2 + k^2 + 2U_{k,\rho}} + \frac{\alpha_2(\omega_n^2)^2 + \alpha_1\omega_n^2 + \alpha_0}{(\omega_n^2)^3 + \beta_2(\omega_n^2)^2 + \beta_1\omega_n^2 + \beta_0} \right), \quad (47)$$

$$\partial_t U_{k,F} = -\frac{8k^5 T}{3\pi^2} \sum_{n \in \mathbb{Z}} \frac{(\nu_n + a_0)^2 + k^2 + g^2\phi^2 - \mu^2}{((\nu_n + a_0)^2 + E_k^{+2})(\nu_n + a_0)^2 + E_k^{-2}}, \quad (48)$$

where we have introduced  $E_k^\pm = \sqrt{g^2 d^2 + (\epsilon_k \pm \mu)^2}$ , and  $\epsilon_k = \sqrt{k^2 + g^2 \rho^2}$  analogous to the notations of Sec. III. The numerator of the second term in the bosonic flow, Eq. (47), is a quadratic polynomial in  $\omega_n^2$  with three coefficient functions  $\alpha_i$ , while the denominator is a cubic polynomial in standard form, with coefficient functions  $\beta_i$  and leading coefficient  $\beta_3 = 1$ . These coefficient functions  $\alpha_i$  and  $\beta_i$  depend on renormalization scale, chemical potential, fields and the derivatives of the potential. They are obtained straightforwardly from the trace of the

inverse of the  $3 \times 3$  submatrix of the bosonic 2-point function in Eq. (45) corresponding to the sigma and diquark directions in field space, and they are listed explicitly in Appendix D for completeness. With the roots of the denominator which we denote as  $\omega_{n,0}^2 = -z_i^2$ ,  $i = 1, \dots, 3$ , we can evaluate all Matsubara sums analytically by virtue of the residue theorem in a standard way.

Hence, the final flow equation for the effective potential of the PQMD model is the sum of the bosonic and fermionic flow and reads explicitly,

$$\partial_t U_k = \frac{k^5}{12\pi^2} \left\{ \frac{3}{E_k^\pi} \coth\left(\frac{E_k^\pi}{2T}\right) + \sum_{i=1}^3 \frac{\alpha_2 z_i^4 - \alpha_1 z_i^2 + \alpha_0}{(z_{i+1}^2 - z_i^2)(z_{i+2}^2 - z_i^2)} \frac{1}{z_i} \coth\left(\frac{z_i}{2T}\right) - \sum_{\pm} \frac{8}{E_k^\pm} \left( 1 \pm \frac{\mu}{\sqrt{k^2 + g^2 \rho^2}} \right) \left( 1 - 2N_q(E_k^\pm; T, \Phi) \right) \right\}, \quad (49)$$

where  $E_k^\pi = \sqrt{k^2 + 2U_{k,\rho}}$ , and  $N_q(E; T, \Phi)$  are the Polyakov loop enhanced quark occupation numbers from Eq. (33). Without a diquark condensate, *i.e.* by setting

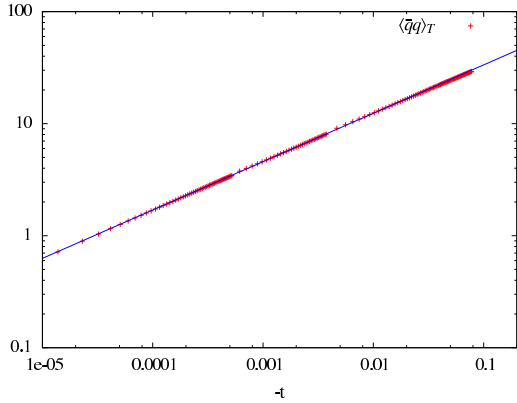
explicitly  $\Delta = 0$ , we can write down an  $SO(6)$ -symmetric flow equation for  $U_k(\phi)$ , if we set  $U_{k,\phi} \equiv U_{k,\rho} = U_{k,d}$ . Eq. (49) then reduces to the more familiar looking form,

$$\partial_t U_k = \frac{k^5}{12\pi^2} \left\{ \frac{3}{E_k^\pi} \coth\left(\frac{E_k^\pi}{2T}\right) + \frac{1}{E_k^\sigma} \coth\left(\frac{E_k^\sigma}{2T}\right) + \frac{1}{E_k^\pi} \coth\left(\frac{E_k^\pi - 2\mu}{2T}\right) + \frac{1}{E_k^\pi} \coth\left(\frac{E_k^\pi + 2\mu}{2T}\right) - \frac{16}{\epsilon_k} \left( 1 - N_q(\epsilon_k - \mu; T, \Phi) - N_q(\epsilon_k + \mu; T, \Phi) \right) \right\}, \quad (50)$$

with single-particle energies for mesons/diquarks  $E_k^\pi = \sqrt{k^2 + 2U_{k,\phi}}$  and sigma  $E_k^\sigma = \sqrt{k^2 + 2U_{k,\phi} + 4\phi^2 U_{k,\phi\phi}}$ . Except for the change in the number of active degrees of freedom contributing to this flow, and the isospin-like chemical potential coupling to one pseudo-Goldstone boson pair, the  $SO(6)$  symmetric flow equation here is entirely analogous the one of the PQM model in the three-color case, see *e.g.*, [48, 64, 65]. For the three-color PQM

model with isospin chemical potential one must allow for pion condensation, however, and then arrives at a flow equation [41] analogous to our Eq. (49).

In the following sections we present numerical solutions to the flow equation (49). The full effective potential depends in general on three condensates which hampers its numerical solution enormously. In order to proceed we restrict ourselves in this work to the two-color QMD

FIG. 6. Fit to chiral condensate for critical exponent  $\beta$ .

model and neglect the influence of the Polyakov-loop by setting  $\Phi = 1$  in the flow and postpone the full PQMD model solution for a later analysis. For the first time we generalize the one-dimensional grid solution technique to two dimensions. Details of the numerical procedure and the parameter fixing can be found in Appendix A.

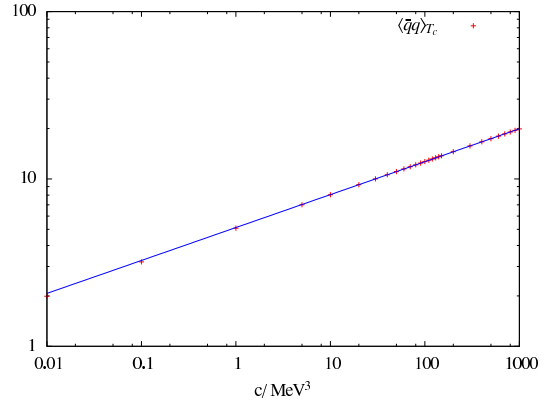
### A. Critical exponents $\beta$ and $\delta$

Without diquark condensation for vanishing chemical potential, and Polyakov-loop variable  $\Phi = 1$ , the  $SO(6)$  symmetric flow in Eq. (50) further simplifies to

$$\partial_t U_k = \frac{k^5}{12\pi^2} \left\{ \frac{5}{E_k^\pi} \coth\left(\frac{E_k^\pi}{2T}\right) + \frac{1}{E_k^\sigma} \coth\left(\frac{E_k^\sigma}{2T}\right) - \frac{16}{\epsilon_k} \tanh\left(\frac{\epsilon_k}{2T}\right) \right\}. \quad (51)$$

At  $\mu = 0$  the diquarks are degenerate with the pions which leaves us with the  $N_c = 2$  analogue of the familiar three-color QM model flow equation [66, 67] except that there are now five pseudo-Goldstone bosons instead of the usual three pions.

The study of  $O(4)$  universality and scaling in the three-color QM model has a long history by now [68–72]. Here we can analogously check the symmetry breaking patterns discussed in Section II A by computing the corresponding critical exponents. As discussed there, for  $\mu = m = 0$ , the  $SU(4) \simeq SO(6)$  dynamically breaks down to  $Sp(2) \simeq SO(5)$  so that we expect a finite temperature phase transition in the three-dimensional  $O(6)$  universality class. The critical exponent  $\beta$  can be extracted from the dependence of the chiral condensate on the reduced temperature  $t = (T - T_c)/T_c$  in the chiral limit, whereas the exponent  $\delta$  governs the dependence of the chiral condensate at  $T_c$  on the quark mass  $m_q$  or correspondingly on the explicit symmetry-breaking pa-

FIG. 7. Fit to chiral condensate for critical exponent  $\delta$ .

rameter  $c$ ,

$$\langle \bar{q}q \rangle_T \sim (-t)^\beta, \quad \langle \bar{q}q \rangle_{T_c} \sim c^{1/\delta}. \quad (52)$$

With the usual two-exponent scaling all other critical exponents are then obtained from these two. Here we find critical exponents  $\beta = 0.4318(4)$  and  $\delta = 5.08(8)$  from the solution of the  $1d$  flow equation (51) via the Taylor expansion method. The given errors are statistical errors extracted from the fit. The corresponding fits are shown in Figs. 6 and 7, respectively. Literature values for these exponents obtained from Monte-Carlo simulations are given by  $\beta = 0.425(2)$  and  $\delta = 4.77(2)$  [73]. At the leading order derivative expansion employed here, we should not expect to reproduce these values, however. The more appropriate benchmark here should be the functional renormalization group result for the  $O(6)$  model in leading order derivative expansion [74]. In absence of wave-function renormalizations there is no anomalous dimension for the fields and their critical exponent therefore vanishes,  $\eta = 0$ . Then the hyperscaling relations,

$$\delta = \frac{d+2-\eta}{d-2+\eta}, \quad \beta = \frac{\nu}{2}(d-2+\eta), \quad (53)$$

immediately entail that  $\delta = 5$  and  $\beta = \nu/2$  in  $d = 3$  dimensions. With the correlation-length critical exponent  $\nu = 0.863076$  from Ref. [74] this corresponds to  $\beta = 0.4315$ , and both our values are in agreement with these two within our errors.

### B. Phase diagram without diquark fluctuations

Before we discuss the solutions to the full flow equation (49) for the effective potential with fluctuations of both condensates included, it might be instructive to illustrate the influence of fluctuations on the standard quark-meson-model-like phase diagram without baryonic

degrees of freedom. The phase diagram obtained from our solutions to the  $SO(6)$ -symmetric flow equation (50) in the  $(T, \mu)$ -plane is compared to the mean-field results from Sec. III A in Fig. 8. The mean-field solutions there were obtained from Eq. (19) with  $d^2 = |\Delta|^2 = 0$  and with a vacuum term cut off at  $\Lambda = 600$  MeV which is sufficiently large for a reasonable comparison, see Sec. III A. The parameters were chosen so as to match the  $\mu = 0$  chiral transition temperatures (rather than the sigma mass) in addition to pion decay constant and pion mass, as explained in Appendix A.

Again, the resulting phase diagram with fluctuations shows the typical form of the QM model for  $N_c = 3$ . It has a critical endpoint at  $\mu \approx 2.5m_\pi$  as compared to that at  $\mu \approx 2.8m_\pi$  in the mean-field calculation. The dotted chiral-crossover lines are again simply the half-value curves of the chiral condensate. Except for the shift of the critical endpoint and the crossover-line in the range of chemical potentials between 2.5 and  $2.8m_\pi$ , the chiral-crossover line from the RG solution closely follows the mean-field result. As discussed in Sec. III B already, they are both equally wrong for baryon chemical potentials of the order of the baryon mass and above, as we have neglected the essential dynamics of the baryonic diquarks in the superfluid phase.

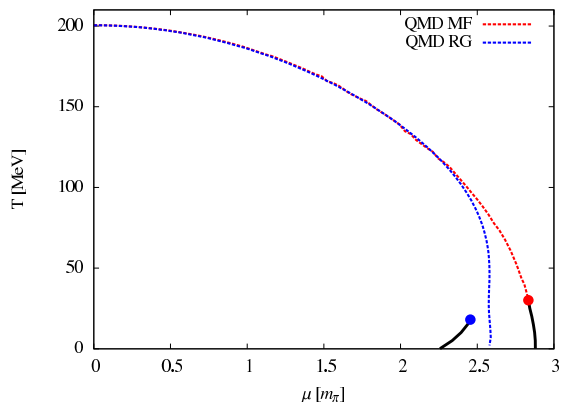


FIG. 8. QMD model phase diagram without baryonic degrees of freedom ( $d = 0$ ): 1d RG result vs. MF ( $\Lambda = 600$  MeV).

The advantage here as compared to the three-color case is that it is much more straightforward to include baryonic degrees of freedom, by properly including the diquarks, both at mean-field level and in the full flow equation (49). All we have to do is to solve this equation in the higher-dimensional space of invariants in the fields representing both possible order parameters and

their fluctuations at the same time.

### C. FRG pole mass and flow of the 2-point function

The fact that the Silver Blaze property links the onset of diquark condensation to the zero-temperature pion mass represents a strong constraint which has to hold in the (P)QMD model with fluctuations also. As we have already illustrated at mean-field level in Section III C, a proper definition of meson and baryon masses is absolutely crucial for this exact property of the theory. In particular, we have seen explicitly that the behavior of widely used screening masses is unphysical in this regard. In the mean-field calculations, the difference between the pion's pole and screening masses at zero temperature and with identical model parameters can be as much as 30%, for example. Adjusting the parameters to the more physical pole mass instead of the common procedure in these models has a considerable influence on the results. So this is more than an academic exercise.

Therefore, we propose a simple procedure to obtain pole masses suitable for the FRG framework: As an extension to the flow equation for the effective potential in the leading order derivative expansion, we solve the flow equations for the 2-point functions of mesons and diquarks using the field and scale dependent but momentum independent 3- and 4-point vertices obtained from the effective potential. This ensures that the flow equations for the 2-point functions at zero momentum reduce to those for the mass terms in the effective potential and that the screening masses obtained from the flows of 2-point functions and effective potential are therefore the same by construction. This truncation for the flow of the 2-point functions most naturally extends that of the effective potential, and thus provides a simple alternative to other approaches such as the BMW approximation [75] where the same relation with the effective potential typically arises as an additional requirement.

In this section we outline the derivation and solution methods for the flow equation of the pion 2-point function  $\Gamma_{\pi\pi}^{(2)}$  at  $T = \mu = 0$  as an example which will allow us to define a pion pole mass in the vacuum. We consider  $N_f$  flavors of quark with  $N_c$  colors coupled to an  $O(N)$ -symmetric bosonic sector for combinations of  $N_f$ ,  $N_c$  and  $N$  where this is possible.

The flow equation for the (field dependent) 2-point function is given by the second functional derivative of the original flow equation (42) which in our case is,

$$\begin{aligned} \partial_t \Gamma_{ij}^{(0,2)}(p; \phi) = & \int \frac{d^4 q}{(2\pi)^4} \partial_t R^B(q)_{kl} \left( G^B(q)_{lm} \Gamma_{mnj}^{(0,3)} G^B(q-p)_{nr} \Gamma_{rsi}^{(0,3)} G^B(q)_{sk} - \frac{1}{2} G^B(q)_{lm} \Gamma_{mni}^{(0,4)} G^B(q)_{nk} \right) \\ & - 2 \text{tr} \partial_t R^F(q) \left( G^F(q) \Gamma_j^{(2,1)} G^F(q-p) \Gamma_i^{(2,1)} G^F(q) - \frac{1}{2} G^F(q) \Gamma_{ij}^{(2,2)} G^F(q) \right), \end{aligned} \quad (54)$$

where  $G^B(p) = (\Gamma_k^{(0,2)}(p; \phi) + R_k^B(p))^{-1}$  and  $G^F(p) = (\Gamma_k^{(2,0)}(p; \phi) + R_k^F(p))^{-1}$ . To solve the flow equation (54) one needs 3<sup>rd</sup> and 4<sup>th</sup> derivatives of  $\Gamma_k[\phi]$  which we denote generically by  $\Gamma_k^{(n,m)}$  where the first(second) superscript counts the number of fermionic(bosonic) derivatives. In order for the limit  $p \rightarrow 0$  to be consistent with the truncation used for the flow equation of the effective potential we obtain those higher  $n$ -point vertex functions from the same scale-dependent effective action. In leading order derivative expansion, Eqs. (44), (49) or (51) for  $\mu = 0$ , the 3- and 4-point functions are then momentum independent, and the only dependence on the external momentum comes from the propagators themselves. For convenience we choose coordinates  $\phi_i = \phi \delta_{i1}$ , *i.e.*,  $\sigma = \phi$  and the others zero, so that one has explicitly for the quark-boson vertices with constant Yukawa couplings,

$$\Gamma_0^{(2,1)} = g, \quad \Gamma_{j \neq 0}^{(2,1)} = ig\gamma^5 \tau_j, \quad \Gamma_{ij}^{(2,2)} = 0. \quad (55)$$

The three and four-boson vertices are extracted from the respective derivatives of the  $k$ -dependent effective poten-

tial  $U_k$ . Here this is a function of  $\phi^2$  and we simply write  $U_k''(\phi^2) \equiv U_{k,\phi\phi}$  etc. instead of our index notation above,

$$\Gamma_{ijm}^{(0,3)} = 4\phi U_k'' (\delta_{ij}\delta_{m1} + \delta_{jm}\delta_{i1} + \delta_{im}\delta_{j1}) + 8\phi^3 U_k^{(3)} \delta_{i1}\delta_{j1}\delta_{m1}, \quad (56)$$

$$\begin{aligned} \Gamma_{ijmn}^{(0,4)} &= 4U_k'' (\delta_{ij}\delta_{mn} + \delta_{in}\delta_{jm} + \delta_{jn}\delta_{im}) \\ &+ 8\phi^2 U_k^{(3)} (\delta_{ij}\delta_{m1}\delta_{n1} + \delta_{jm}\delta_{i1}\delta_{m1} + \delta_{mn}\delta_{i1}\delta_{j1} \\ &\quad + \delta_{jn}\delta_{i1}\delta_{m1} + \delta_{in}\delta_{j1}\delta_{m1}) \\ &+ 16\phi^4 U_k^{(4)} \delta_{i1}\delta_{j1}\delta_{m1}\delta_{n1}. \end{aligned} \quad (57)$$

For the calculation of the boson masses we use their rest frame, setting the spatial external momentum  $\vec{p} = 0$  in Eq. (54). In this frame the spatial momentum integrals with the optimized regulators are still trivially performed. Evaluating the flow equation (54) one obtains after analytically continuing  $p_0 = -i\omega$ , and with the same notations  $\Gamma^{(0,2)}(\omega) \equiv \Gamma^{(0,2)}(p = (-i\omega, \vec{0}); \phi)$  as in Sec. III C above,

$$\begin{aligned} \partial_t \Gamma_{k,\pi\pi}^{(0,2)}(\omega) &= \frac{k^5}{6\pi^2} \left( -\frac{(N+1)U_k''}{E_k^{\pi^3}} + \frac{2U_k''(E_k^{\sigma^2} - E_k^{\pi^2})}{E_k^{\pi^3} E_k^{\sigma^3} ((E_k^{\pi^2} + E_k^{\sigma} E_k^{\pi} + E_k^{\sigma^2}) - (E_k^{\sigma^3} + E_k^{\pi^3})\omega^2)} \right. \\ &\quad \left. - \frac{U_k'' + 2\phi^2 U_k^{(3)}}{E_k^{\sigma^3}} + \frac{8N_f N_c g^2 (4\epsilon_k^2 + \omega^2)}{\epsilon_k (4\epsilon_k^2 - \omega^2)^2} \right). \end{aligned} \quad (58)$$

We set  $\Gamma_{\Lambda,\pi\pi}^{(0,2)}(\omega) \equiv -\omega^2 + 2U'_{k=\Lambda}(\phi^2) = -\omega^2 + \lambda(\phi^2 - v^2)$  at the UV scale  $k = \Lambda$ , and obtain the pion pole mass  $m_{\pi,\text{pole}}$  for  $k \rightarrow 0$  from the condition

$$\Gamma_{k=0,\pi\pi}^{(0,2)}(m_{\pi,\text{pole}}^2) = 0, \quad (59)$$

evaluated at the minimum of the full effective potential. For vanishing external momentum the two-point function can equally be obtained from the second derivative of the effective potential. Indeed, one verifies that the flow equation (58) obeys the consistency condition

$$\partial_t \Gamma_{k,\pi\pi}^{(0,2)}(0) = \frac{\delta_{ij}}{N-1} \frac{\partial^2}{\partial \pi_i \partial \pi_j} \partial_t U_k = 2 \frac{\partial}{\partial \phi^2} \partial_t U_k. \quad (60)$$

This implies that if we calculate  $\Gamma_{k=0,\pi\pi}^{(0,2)}$  by integrating the flow equation (58) for  $\omega = 0$ , the mass defined as

$$m_{\pi}^{\text{sc}2} = \Gamma_{k=0,\pi\pi}^{(0,2)}(0) \quad (61)$$

correspondingly, simply represents the same screening mass as obtained from the curvature of the effective potential at its minimum, which is usually considered in QM model calculations within the FRG framework.

The flow equation (58) can be solved via a Taylor expansion method around a scale dependent expansion

point for both the effective potential and the two-point function, or on a grid in field space. In order to maintain the relation in Eq. (60) also in the numerical calculations based on Taylor expansions in  $\phi^2$ , one has to use one expansion order less for the 2-point function than for the effective potential. In this way we can compute an estimate of the pion pole mass from a given UV potential.

Table I shows a comparison of screening and pole masses as obtained from the Taylor and grid methods. All calculations here were performed at  $T = \mu = 0$ . As explained in Sec. III C and Appendix A, we have adjusted the start parameters for the flow in our two-dimensional grid code to fix the onset of diquark condensation to occur at  $2\mu_c \approx 138$  MeV which defines the physical pion mass in the normal phase. The exact same parameters were used to obtain the UV forms of effective potential and inverse propagators for the one-dimensional Taylor expansion method at  $\mu = 0$ . The results from one- and two-dimensional grid computations at  $\mu = 0$  are indistinguishable at this level of accuracy, as are the screening masses from Eq. (61) and from the effective potential. The slight deviations in  $f_{\pi}$  and the masses in Table I between the grid and Taylor methods are an indication of the small residual uncertainties.

With the onset at half the physical pion mass fixed,

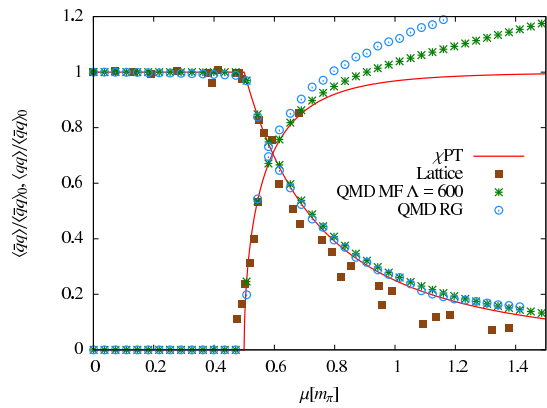


FIG. 9. Zero temperature condensates from full flow compared to mean-field results (and the lattice data from [17]).

we then observe that the standard screening masses generally overestimate the pion mass by about 30%. In contrast, our pion pole mass estimates based on solving Eqs. (58) and (59) lie within 11%, but they are smaller than the physical one.

The extrapolation from zero pion momentum in the leading order derivative expansion to the pion pole in the propagator from our consistent truncation scheme appears to be too large, so that it overcompensates the difference between onset and screening mass. In order to disentangle the effect of bosonic and fermionic contributions to the flow equation (58) for the pion 2-point function, we have also solved this equation with  $\omega = 0$  in the bosonic and in the fermionic parts, separately. The resulting pole masses are denoted by  $m_{\pi,\text{pole, ferm. only}}$

method	quantity	value[MeV]
Grid	$f_{\pi}$	76.0
	$m_{\pi,\text{scr}}$	178.8
	$m_{\sigma,\text{scr}}$	551.7
	$2\mu_c$	<b>137.8</b>
	$m_{\pi,\text{pole}}$	<b>122.45</b>
	$m_{\pi,\text{pole, ferm. only}}$	124.9
	$m_{\pi,\text{pole, bos. only}}$	171.6
Taylor	$f_{\pi}$	75.0
	$m_{\pi,\text{scr}}$	180.0
	$m_{\sigma,\text{scr}}$	550.8
	$m_{\pi,\text{pole}}$	<b>122.6</b>
	$m_{\pi,\text{pole, ferm. only}}$	125.0
	$m_{\pi,\text{pole, bos. only}}$	172.6

TABLE I. Comparison of RG screening vs. pole masses; ‘ferm. only’ (‘bos. only’) refers to maintaining only the constant  $\omega = 0$  contributions in the bosonic (fermionic) contribution to the flow of the pion 2-point function, Eq. (58).

and  $m_{\pi,\text{pole, bos. only}}$  in Table I, respectively. Both contributions reduce the screening masses, but the fermions clearly generate the dominant effect. This suggests that one might have to go beyond the leading-order derivative expansion employed here and allow for an RG flow of the Yukawa couplings by including field renormalizations and anomalous dimensions [76].

#### D. Phase diagram of the QMD model for two-color QCD with mesonic and baryonic fluctuations

In Fig. 9 we show once more the dependence of the chiral and diquark condensates on the chemical potential at zero temperature as in Fig. 3, but this time with including our results from the full RG solution to Eq. (49) on a two-dimensional grid in field space with  $\Phi = 1$ .

The final effect of baryonic-diquark degrees of freedom is illustrated in Fig. 10 where we compare the phase diagram from the one-dimensional RG flow solution to the  $SO(6)$ -symmetric equation (50) from Sec. IV B and that from the full two-dimensional one for an effective potential with the reduced  $SO(4) \times SO(2)$  symmetry.

This clearly illustrates the effect of the competing dynamics of the collective mesonic and baryonic fluctuations. As before, the dashed lines in Fig. 10 indicate the chiral crossover by tracing the half-value of the chiral condensate. Both, the one and the two-dimensional results agree for quark-chemical potentials near zero. The crossover in this region leads to mesonic freeze-out as usual, and the results are unambiguously determined by the  $O(6)$  symmetry breaking pattern, see Sec. IV A. Allowing additional interactions with lower symmetry has no effect on the flow here.

Once the quark-chemical potential approaches half the baryon mass, corresponding to  $m_B/N_c$ , however, the rapidly increasing baryon density equally rapidly suppresses the chiral condensate. With the proper inclusion of the collective baryonic excitations, there is no trace left of the chiral first-order transition and the critical endpoint of the purely mesonic model. The baryon density is an order parameter for  $N_f = N_c = 2$ , and the transition line would be expected to give rise to the two-color analogue of the baryonic freeze-out.

The onset of diquark condensation and superfluidity of our bosonic baryons, with  $SO(3) \times SO(2) \rightarrow SO(3)$  symmetry breaking at finite quark mass and chemical potential, also marks the line at which the the residual  $SO(3)$  symmetry starts changing in nature from an approximate  $SO(5)$  symmetry as in the normal phase to becoming the approximate  $SO(4) \simeq SU(2)_L \times SU(2)_R$  quasi-restored chiral symmetry. Because they are both explicitly broken and only approximate symmetries, this vacuum realignment naturally is a crossover. The quark mass with large chiral condensate in the normal phase starts out as a predominantly spontaneously generated Dirac mass, and the bosonic baryons undergo Bose-Einstein condensation as a dilute gas of strongly bound diquarks with the onset

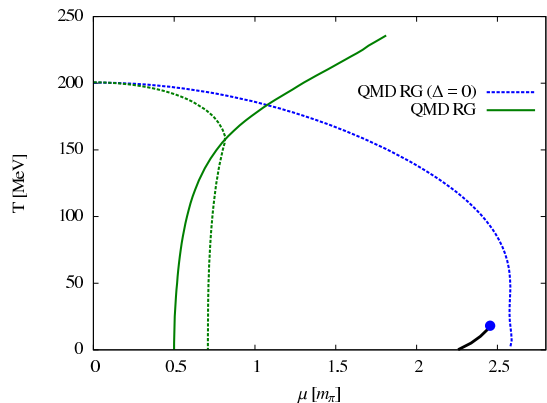


FIG. 10. Phase diagram from RG flow with collective baryonic fluctuations (and no chiral 1<sup>st</sup> order transition/critical endpoint) compared to the purely mesonic model ( $\Delta = 0$ ).

of diquark superfluidity. As their density increases, the underlying quark mass rotates into a spontaneous Majorana mass leading to a BCS-like pairing. This is the relativistic analogue in two-color QCD of the BEC-BCS crossover observed in ultracold fermionic quantum gases. It is indicated in Fig. 11 as additional dashed lines in the superfluid phase tracing the lines where the quarks' Dirac-mass  $m_q = g\sigma$  equals their chemical potential, *i.e.*  $\mu = m_q$ , see [32] for a comprehensive discussion of this crossover within the NJL model.

In this Figure 11 we compare the phase diagram of the QMD model for two-color QCD as obtained from the full RG solution with the mean-field result of Sec. III B. The line of the diquark-condensation phase transition, which one expects to be of  $O(2)$ -universality, in the QMD model RG solution with fluctuations differs more and more from that obtained in mean-field QMD and NJL model calculations as temperature increases. The first-order transition line is washed out by the fluctuations and the associated tricritical point as also predicted from next-to-leading order  $\chi$ PT [9] turns out to be a mean-field artifact. As already visible from the  $T = 0$  results for the condensates, *c.f.* Fig. 9, the phase diagrams approach one another at small temperatures.

## V. SUMMARY AND OUTLOOK

In this paper we have developed a Polyakov-loop extended quark-meson-diquark model for two-color QCD and derived the functional renormalization group equation for the grand potential in the leading-order derivative expansion. We discussed the mean-field thermodynamics of the model and solved the RG flow equation for trivial Polyakov-loop, *i.e.* for the corresponding quark-meson-diquark model. In order to correctly describe the competing dynamics of collective mesonic and baryonic

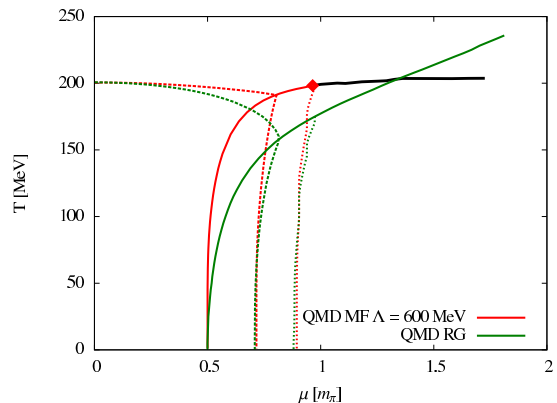


FIG. 11. Comparison of QMD phase diagrams from MF and RG calculations, including lines with  $g\sigma = \mu$  in the superfluid phase to indicate the BEC-BCS crossover.

diquark fluctuations, it is thereby necessary to introduce two invariants of the fields in order to account for the rich symmetry and symmetry-breaking structure of two-color QCD as reviewed in our introduction. The functional RG for the effective potential then describes the interplay between the collective mesonic and baryonic (diquark) fluctuations as summarized once more with showing the resulting chiral and diquark condensates over temperature and quark chemical potential in a three-dimensional plot in Fig. 12. Our numerical solution method on a higher-dimensional grid in field space represents important technical progress with many further applications.

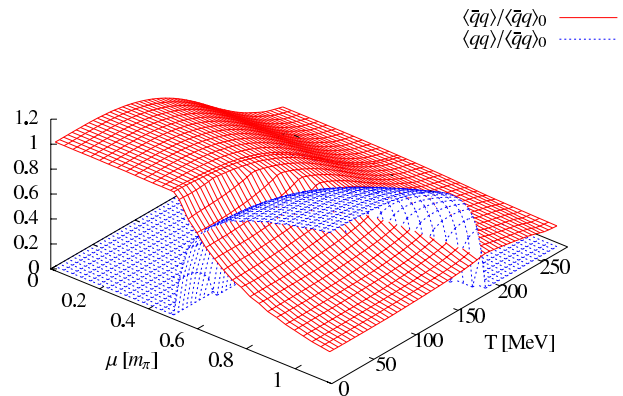


FIG. 12. Summary: Chiral condensate and diquark condensate as function of temperature and chemical potential from RG calculation.

One particular advantage of using two instead of the usual three colors is that our non-perturbative functional methods and model results can be tested against exact results and lattice simulations in two-color QCD. First important results from such tests are: The expected  $O(6)$  scaling at zero density; the relevance of pole masses in the

RG framework to correctly describe the onset of diquark condensation at the zero temperature quantum phase transition of two-color QCD, and the failure of the usual screening masses to be capable of that; and finally but most importantly, the non-existence of a chiral first-order transition and critical endpoint at finite baryon density.

The latter is not surprising for two-color QCD alone, with the BEC-BCS crossover in the superfluid phase of the bosonic baryons. We argue, however, that our comparison between the full results with inclusion of collective baryonic excitations and the corresponding purely mesonic model reveals a general effect, relevant to the real world: the chiral condensate drops discontinuously at the low temperature liquid-gas transition to nuclear matter, and it will continue to decrease with increasing baryon density so that one might question whether there will be enough chiral-symmetry breaking left for a another first-order transition at the expected higher densities. Similarly, one might speculate that the second-order phase-transition line of two-color QCD to diquark superfluidity at finite temperature would lead to the analogue of the observed baryonic freeze-out line in the region of rapidly increasing baryon density in real QCD.

Another advantage is that the proper inclusion of baryonic degrees of freedom is much more straightforward and much simpler here as in real QCD. While this is to a large extent due to the fact that those baryons are represented by bosonic diquarks, our study of two-color QCD can serve as an important first step towards including diquark-correlations and explicit baryonic degrees of freedom in a covariant quark-diquark description by a corresponding quark-meson-baryon model for QCD.

More tests of refined truncations will be performed in the future, including a dynamical coupling of the quark-meson-diquark model studied here to the full gauge-field dynamics of two-color QCD along the lines of what has been done already without explicit baryonic contributions for QCD [78, 79].

## ACKNOWLEDGMENTS

The authors thank Tomáš Brauner, Michael Buballa, Holger Gies, Kazuhiko Kamikado, Mario Mitter, Jan Pawłowski, David Scheffler and Jochen Wambach for useful discussions. This work was supported by the Helmholtz International Center for FAIR within the LOEWE program of the State of Hesse, the Helmholtz Association Grant VH-NG-332, and the European Commission, FP7-PEOPLE-2009-RG No. 249203.

## Appendix A: Parameter fixing and numerical procedure

In this appendix we briefly outline our parameter fitting and the numerical methods for the solution of the flow equation.

Since two-color QCD is an unrealistic theory there is no canonical choice to fix the parameters to measurable quantities. A common approach, often found in the literature, is to use the experimentally known  $N_c = 3$  values and their  $N_c$  scaling to obtain a consistent  $N_c = 2$  parameter set. Therefore the assumption  $f_\pi \sim \sqrt{N_c}$  yields  $f_\pi = 76$  MeV if the usual three-color value  $f_\pi^{(3)} = 93$  MeV is chosen. Furthermore, we assume that the vacuum pion and sigma masses do not scale with  $N_c$  and fix the pion mass to  $m_\pi = m_{\pi,0} = 138$  MeV.

As pointed out above the mass definition at mean-field level which is consistent with the Silver Blaze property is the pole mass defined via Eq. (34). Usually, in QM studies we fix  $\sigma(T = \mu = 0) = f_\pi$  together with the pion and the sigma masses in the vacuum. The pion and sigma pole mass equations Eq. (34) fix the constants  $\lambda$  and  $v^2$  in the potential  $V = \frac{\lambda}{4}(\phi^2 - v^2)^2 - c\sigma$ . The explicit symmetry breaking constant  $c$  is then determined by the gap equation. In this way the parameters  $\lambda$ ,  $v^2$  and  $c$  are found for a fixed momentum cutoff  $\Lambda$  in the vacuum term. As argued above the cutoff  $\Lambda$  should be chosen larger than the largest value of the chemical potential we are interested in. Here we choose  $\Lambda = 600$  MeV and for comparison  $\Lambda = 0$  MeV and adjust  $m_\sigma$  such that the crossover temperature at  $\mu = 0$  coincides with the RG calculation. In Table II we summarize our used parameter values.

$\Lambda$ [MeV]	$m_\sigma$ [MeV]	$g$	$\lambda$	$v^2$ [ $10^3$ MeV $^2$ ]	$c$ [ $10^6$ MeV $^3$ ]
600	680	4.8	25.05	-42.710	2.885
0	1055	4.8	94.70	5.575	1.447

TABLE II. Parameter values in mean-field approximation

In the RG setting we adjust the parameter  $\lambda$  in the UV potential and the explicit symmetry breaking parameter  $c$  while keeping  $v^2 = 0$  in the UV potential and a Yukawa coupling  $g = 4.8$  to match  $f_\pi$  and  $m_\pi$  in the IR. As there are remaining uncertainties in the determination of the pion pole mass via the flow of 2-point function as explained in Sec. IV C, we rather determine  $m_\pi$  via the onset of diquark condensation at  $T = 0$ .

Finally, we point out some details on the numerical procedure to solve the flow equations. The structure of the  $d = 0$  flow (50) and the full flow for  $\mu = 0$ , Eq. (51), is identical to the flow of the usual three-color QM model [67, 70]. Several solution methods such as the finite difference approach, the Taylor expansion of the effective potential around a scale dependent minimum or grid techniques where higher order derivative terms are eliminated algebraically are known which all produce consistent results. For the full flow equation (49) the situation is more

involved since the effective potential is parametrized by two invariants  $U_k = U_k(\rho^2, d^2)$ .

Here we apply a modified grid algorithm where the higher derivatives on the RHS of the flow equation are obtained by a two-dimensional-spline fit of the effective potential at the respective grid point. The numerical results obtained from this procedure agree very well with those from an algorithm where the derivatives were approximated by finite differences at a fixed discretization order.

## Appendix B: Proper-time flow equations

In this appendix we sketch an alternative derivation of the QMD flow equation Eq. (49) with a proper-time regularization, see also [60, 69, 80] and references therein for a short introduction and comparison of the proper-time with the Wetterich flow.

Originally, the proper-time renormalization group equation (PTRG) was found by an RG improvement of a proper-time regularized one-loop effective action [69, 83]. Later, it turned out [81] that the PTRG flow can be related to the Wetterich flow with the background field formalism. The standard PTRG flow can be derived from the Wetterich flow when terms proportional to  $\partial_t \Gamma_k^{(2)}$  are neglected. The PTRG flow for the QMD model splits into a bosonic and fermionic flow  $\partial_t \Gamma_k = \partial_t \Gamma_{k,B} + \partial_t \Gamma_{k,F}$  where  $t = \ln(k/\Lambda)$  denotes the logarithmic RG scale. The one-loop expression can be rewritten via Schwinger's proper-time representation as

$$\begin{aligned} \partial_t \Gamma_k &= -\frac{1}{2} \text{Tr} \int_0^\infty \frac{d\tau}{\tau} \partial_t f_a(\tau k^2) \\ &\left[ \exp\left(-\tau \Gamma_{k,B}^{(2)}\right) - \exp\left(-\tau \Gamma_{k,F}^{(2)}(\mu) \Gamma_{k,F}^{(2)\dagger}(-\mu)\right) \right], \end{aligned} \quad (\text{B1})$$

where the trace runs over momenta and internal indices.<sup>2</sup> As before, the second functional derivative of effective action with respect to bosonic(fermionic) fields is denoted by  $\Gamma_{k,B}^{(2)}$  ( $\Gamma_{k,F}^{(2)}$ ). The proper-time regulator function  $f_a(\tau k^2)$  has to fulfill some constraints and the optimal choice, based on incomplete Gamma functions, is  $f_a(\tau k^2) = \Gamma(a+1, \tau k^2)/\Gamma(a+1)$  with  $a = 3/2$  which can also be mapped to the optimized regulator in the Wetterich flow, for details see [82].

In the bosonic case  $\Gamma_{k,B}^{(2)}$  is given by Eq. (45) and can be diagonalized. Three of the six eigenvalues which are related to the three massless pions are degenerate and

<sup>2</sup> For the fermionic part we make use of  $\gamma_5$  hermiticity and parity invariance of the Dirac operator by writing (using the notation of Eq. (12))  $A^5 \Gamma_{F,k}^{(2)}(\sigma, \vec{\pi}, \Delta; \mu) A^5 = \Gamma_{F,k}^{(2)\dagger}(\sigma, -\vec{\pi}, \Delta; -\mu) = \Gamma_{F,k}^{(2)\dagger}(\sigma, \vec{\pi}, \Delta; -\mu)$  with  $A^5 = \begin{pmatrix} \gamma_5 & 0 \\ 0 & -\gamma_5 \end{pmatrix}$ .

read explicitly  $\vec{p}^2 + \lambda_{n,k}^{(i)} = \vec{p}^2 + \omega_n^2 + 2U_{k,\rho}$ ,  $i = 1, 2, 3$  where  $\omega_n = 2\pi nT$  are the bosonic Matsubara frequencies. The remaining three eigenvalues  $\vec{p}^2 + \lambda_{n,k}^{(i)}$ ,  $i = 4, 5, 6$  are more complicated and are related to the radial  $\sigma$ -meson and the two diquarks. The three-momentum integration separates and can be done analytically. After the proper-time integration the bosonic flow is composed of a sum over all eigenvalues

$$\partial_t \Gamma_{k,B} = \frac{T}{3} \frac{k^5}{2\pi^2} \sum_{i=1}^6 \sum_{n \in Z} \frac{1}{k^2 + \lambda_{n,k}^{(i)}}. \quad (\text{B2})$$

Rewriting

$$\sum_{i=4}^6 \frac{1}{k^2 + \lambda_{n,k}^{(i)}} = \frac{\alpha_2(\omega_n^2)^2 + \alpha_1\omega_n^2 + \alpha_0}{(\omega_n^2)^3 + \beta_2(\omega_n^2)^2 + \beta_1\omega_n^2 + \beta_0} \quad (\text{B3})$$

with the  $k$ - and  $\mu$ -dependent coefficient functions  $\alpha_l$  and  $\beta_l$  listed explicitly in Appendix D we arrive at the bosonic flow equation Eq. (47) again.

In the fermionic sector including the coupling to the gauge field via the Polyakov loop variable  $\Phi = \cos(\beta a_0)$  we find two  $4N_f (= 8)$ -fold degenerate eigenvalues  $\lambda_{n,k}^\pm$  of the matrix  $\Gamma_{k,F}^{(2)}(\mu) \Gamma_{k,F}^{(2)\dagger}(-\mu)$

$$\lambda_{n,k}^\pm = (\nu_n + a_0)^2 - \mu^2 + g^2 \phi^2 \pm 2i\mu \sqrt{(\nu_n + a_0)^2 + g^2 |\Delta|^2}, \quad (\text{B4})$$

with the fermionic Matsubara frequencies  $\nu_n = (2n + 1)\pi T$ . This thus yields the fermionic flow of the effective potential

$$\begin{aligned} \partial_t \Gamma_{k,F} &= -\frac{4Tk^5}{3\pi^2} \sum_{j=\pm} \sum_{n \in Z} \frac{1}{k^2 + \lambda_{n,k}^j} \\ &= -\frac{8k^5 T}{3\pi^2} \sum_{n \in Z} \frac{k^2 + g^2 \phi^2 - \mu^2 + (\nu_n + a_0)^2}{\left((\nu_n + a_0)^2 + E_k^{+2}\right) \left((\nu_n + a_0)^2 + E_k^{-2}\right)}, \end{aligned} \quad (\text{B5})$$

which reproduces Eq. (48). Evaluating the Matsubara sums and combining both contributions then leads to the flow equation (49).

## Appendix C: RPA Meson/Diquark polarization functions

For convenience we indicate the explicit expressions for the meson/diquark polarization functions for vanishing spatial external momentum. These can be calculated most conveniently using massive energy projectors [39]. The Polyakov-loop enhanced quark/antiquark occupation numbers  $N_q$  are defined in Eq. (33) and reduce to the Fermi Dirac distribution for  $\Phi = 1$ . To comply with conventions in the literature the polarization functions are given in a complex basis  $\phi = (\sigma, \vec{\pi}, \Delta, \Delta^*)$  and correspondingly with Eq. (29) replaced by

$$\Pi_{ij}(p) = \text{Tr}_q \left[ \frac{\partial \Gamma_F^{(2)}}{\partial \phi_i^*} \Big|_{\phi_{\text{MF}}} G_{\text{MF}}(p+q) \frac{\partial \Gamma_F^{(2)}}{\partial \phi_j} \Big|_{\phi_{\text{MF}}} G_{\text{MF}}(q) \right]. \quad (\text{C1})$$

There is a subtlety concerning the  $\omega \rightarrow 0$  limit at finite temperature  $T > 0$  as mentioned in Sec. III C. The standard procedure within the imaginary-time formalism assumes that the external Euclidean  $p_0 = -i\omega$  is a discrete Matsubara frequency  $2\pi nT$  ( $n \in \mathbb{Z}$ ). One then assumes additional analyticity properties to define a unique analytic continuation. The polarization functions are then singular in the origin of momentum space and one needs to maintain a finite spatial external momentum  $\vec{p}$  to define dynamic screening masses via the limit

$|\vec{p}| \rightarrow 0$  at  $\omega = 0$ . This leads to a discontinuity at  $\omega = 0$  and gives rise to additional contributions  $\delta_{\omega,0}\Pi_{ij}^0$  for the zero mode  $\omega = 0$  (see below). Note that polarization functions for Goldstone and would-be-Goldstone modes are protected from these contributions  $\delta_{\omega,0}\Pi^0$ , *i.e.*, only  $\Pi_{\sigma\sigma}^0$  is nonzero in the normal phase. Using  $m_q = g\sigma$  and  $\epsilon_q = \sqrt{\vec{q}^2 + m_q^2}$ ,  $\epsilon_q^\pm = \epsilon_q \pm \mu$ ,  $E_q^\pm = \sqrt{\epsilon_q^{\pm 2} + g^2 d^2}$  as in Eqs. (18) the polarization functions are given by<sup>3</sup>

$$\begin{aligned} \Pi_{\pi_i\pi_j}(\omega, T) = & -4N_c g^2 \delta_{ij} \int \frac{d^3q}{(2\pi)^3} \left[ \frac{E_q^+ E_q^- - \epsilon_q^+ \epsilon_q^- - g^2 d^2}{\omega^2 - (E_q^- - E_q^+)^2} \left( \frac{1}{E_q^+} - \frac{1}{E_q^-} \right) (N_q(E_q^-) - N_q(E_q^+)) \right. \\ & \left. - \frac{E_q^+ E_q^- + \epsilon_q^+ \epsilon_q^- + g^2 d^2}{\omega^2 - (E_q^- + E_q^+)^2} \left( \frac{1}{E_q^+} + \frac{1}{E_q^-} \right) (1 - N_q(E_q^-) - N_q(E_q^+)) \right], \end{aligned} \quad (C2)$$

$$\begin{aligned} \Pi_{\sigma\sigma}(\omega, T) = & -4N_c g^2 \delta_{ij} \int \frac{d^3q}{(2\pi)^3} \frac{\vec{q}^2}{\epsilon_q^2} \left[ \frac{E_q^+ E_q^- - \epsilon_q^+ \epsilon_q^- - g^2 d^2}{\omega^2 - (E_q^- - E_q^+)^2} \left( \frac{1}{E_q^+} - \frac{1}{E_q^-} \right) (N_q(E_q^-) - N_q(E_q^+)) \right. \\ & \left. - \frac{E_q^+ E_q^- + \epsilon_q^+ \epsilon_q^- + g^2 d^2}{\omega^2 - (E_q^- + E_q^+)^2} \left( \frac{1}{E_q^+} + \frac{1}{E_q^-} \right) (1 - N_q(E_q^-) - N_q(E_q^+)) \right] \\ & + 4N_c g^2 \int \frac{d^3q}{(2\pi)^3} \frac{m_q^2}{\epsilon_q^2} \sum_{\pm} \left[ \frac{2g^2 d^2}{\omega^2 - 4E_q^{\pm 2}} \frac{1}{E_q^{\pm}} (1 - 2N_q(E_q^{\pm})) \right] + \delta_{\omega,0}\Pi_{\sigma\sigma}^0(T), \end{aligned} \quad (C3)$$

$$\Pi_{\Delta\Delta}(\omega, T) = \Pi_{\Delta^*\Delta^*}(-\omega, T) = 4N_c g^2 \int \frac{d^3q}{(2\pi)^3} \sum_{\pm} \left[ \frac{E_q^{\pm 2} + \epsilon_q^{\pm 2} \mp \omega \epsilon_q^{\pm}}{\omega^2 - 4E_q^{\pm 2}} \frac{1}{E_q^{\pm}} (1 - 2N_q(E_q^{\pm})) \right] + \delta_{\omega,0}\Pi_{\Delta\Delta}^0(T), \quad (C4)$$

$$\Pi_{\Delta\Delta^*}(\omega, T) = \Pi_{\Delta^*\Delta}(\omega, T) = -4N_c g^2 \int \frac{d^3q}{(2\pi)^3} \sum_{\pm} \left[ \frac{g^2 d^2}{\omega^2 - 4E_q^{\pm 2}} \frac{1}{E_q^{\pm}} (1 - 2N_q(E_q^{\pm})) \right] + \delta_{\omega,0}\Pi_{\Delta\Delta^*}^0(T), \quad (C5)$$

$$\begin{aligned} \Pi_{\sigma\Delta}(\omega, T) = \Pi_{\Delta\sigma}(\omega, T) = \Pi_{\sigma\Delta^*}(-\omega, T) = \Pi_{\Delta^*\sigma}(-\omega, T) \\ = 2\sqrt{2}N_c g^2 \int \frac{d^3q}{(2\pi)^3} \frac{gd m_q}{\epsilon_q} \sum_{\pm} \left[ \frac{2\epsilon_q^{\pm} \pm \omega}{\omega^2 - 4E_q^{\pm 2}} \frac{1}{E_q^{\pm}} (1 - 2N_q(E_q^{\pm})) \right] + \delta_{\omega,0}\Pi_{\sigma\Delta}^0(T), \end{aligned} \quad (C6)$$

with additional contributions for  $\omega = 0$  of the form,

$$\Pi_{\sigma\sigma}^0(T) = -g^2 N_c \int \frac{d^3q}{(2\pi)^3} \sum_{\pm} \frac{m_q^2}{\epsilon_q^2} \left( \frac{E_q^{\pm 2} + \epsilon_q^{\pm 2} - g^2 d^2}{E_q^{\pm 2}} \right) (-2N'_q(E_q^{\pm})), \quad (C7)$$

$$\Pi_{\Delta\Delta}^0(T) = \Pi_{\Delta^*\Delta^*}^0(T) = -2N_c g^2 \int \frac{d^3q}{(2\pi)^3} \sum_{\pm} \left( \frac{E_q^{\pm 2} - \epsilon_q^{\pm 2}}{E_q^{\pm 2}} \right) (-2N'_q(E_q^{\pm})), \quad (C8)$$

$$\Pi_{\Delta\sigma}^0(T) = \Pi_{\Delta^*\sigma}^0(T) = \Pi_{\sigma\Delta}^0(T) = \Pi_{\sigma\Delta^*}^0(T) = -2\sqrt{2}N_c g^2 \int \frac{d^3q}{(2\pi)^3} \sum_{\pm} \frac{gd m_q}{\epsilon_q} \frac{\epsilon_q^{\pm}}{E_q^{\pm 2}} (-2N'_q(E_q^{\pm})), \quad (C9)$$

$$\Pi_{\Delta\Delta^*}^0(T) = \Pi_{\Delta^*\Delta}^0(T) = -2N_c g^2 \int \frac{d^3q}{(2\pi)^3} \sum_{\pm} \frac{g^2 d^2}{E_q^{\pm 2}} (-2N'_q(E_q^{\pm})). \quad (C10)$$

<sup>3</sup> Note that apart from the missing zero-mode contributions  $\delta_{\omega,0}\Pi_{ij}^0$ , the prefactor of the terms proportional to  $m_q^2$  in  $\Pi_{\sigma\sigma}$  in the last line of Eq. (C3) differs by a factor of 2 from the corresponding terms given in [39, 40].

The additional contributions  $\Pi_0(T)$  vanish for  $T \rightarrow 0$  but are required to ensure consistency with the screening

mass definition from the effective potential at finite  $T$ , *c.f.* Eqs. (36) and (37).

#### Appendix D: Coefficients in the bosonic flow equation

In this appendix we list the expressions for the coefficient functions  $\alpha_i$  and  $\beta_i$  appearing in Eq. (49).

$$\begin{aligned} \alpha_0 = & 3k^4 + 4k^2(-4\mu^2 + 2U_{k,d} + 2d^2U_{k,dd} + U_{k,\rho} + 2\rho^2U_{k,\rho\rho}) \\ & + 4(4\mu^4 + U_{k,d}^2 + 2U_{k,d}(d^2U_{k,dd} + U_{k,\rho} + 2\rho^2U_{k,\rho\rho}) - 4\mu^2(U_{k,d} + d^2U_{k,dd} + U_{k,\rho} + 2\rho^2U_{k,\rho\rho}) \\ & + 2d^2(U_{k,dd}U_{k,\rho} - 2\rho^2U_{k,\rho d}^2 + 2\rho^2U_{k,dd}U_{k,\rho\rho})) \end{aligned} \quad (D1)$$

$$\alpha_1 = 6k^2 + 8U_{k,d} + 8d^2U_{k,dd} + 4U_{k,\rho} + 8\rho^2U_{k,\rho\rho} \quad (D2)$$

$$\alpha_2 = 3 \quad (D3)$$

$$\begin{aligned} \beta_0 = & (k^2 - 4\mu^2 + 2U_{k,d})(k^4 + 2k^2(-2\mu^2 + U_{k,d} + 2d^2U_{k,dd} + U_{k,\rho} + 2\rho^2U_{k,\rho\rho}) \\ & + 4(-2\mu^2U_{k,\rho} + U_{k,d}U_{k,\rho} + 2d^2U_{k,dd}U_{k,\rho} - 4d^2\rho^2U_{k,\rho d}^2 + 2\rho^2(-2\mu^2 + U_{k,d} + 2d^2U_{k,dd})U_{k,\rho\rho})) \end{aligned} \quad (D4)$$

$$\begin{aligned} \beta_1 = & 3k^4 + 4k^2(2U_{k,d} + 2d^2U_{k,dd} + U_{k,\rho} + 2\rho^2U_{k,\rho\rho}) \\ & + 4(4\mu^4 + U_{k,d}^2 - 4\mu^2(U_{k,d} + d^2U_{k,dd} - U_{k,\rho} - 2\rho^2U_{k,\rho\rho}) + 2U_{k,d}(d^2U_{k,dd} + U_{k,\rho} + 2\rho^2U_{k,\rho\rho}) \\ & + 2d^2(U_{k,dd}U_{k,\rho} - 2\rho^2U_{k,\rho d}^2 + 2\rho^2U_{k,dd}U_{k,\rho\rho})) \end{aligned} \quad (D5)$$

$$\beta_2 = 3k^2 + 8\mu^2 + 4U_{k,d} + 4d^2U_{k,dd} + 2U_{k,\rho} + 4\rho^2U_{k,\rho\rho} \quad (D6)$$

- 
- [1] P. Braun-Munzinger and J. Wambach, *Rev. Mod. Phys.* **81** (2009) 1031.
- [2] B. Friman, C. Hohne, J. Knoll, S. Leupold, J. Randrup, R. Rapp and P. Senger, *Lect. Notes Phys.* **814** (2011) 1.
- [3] L. McLerran, R. D. Pisarski, *Nucl. Phys.* **A796** (2007) 83-100. [arXiv:0706.2191 [hep-ph]].
- [4] Y. Hidaka, L. D. McLerran, R. D. Pisarski, *Nucl. Phys.* **A808** (2008) 117-123. [arXiv:0803.0279 [hep-ph]].
- [5] A. Andronic *et al.*, *Nucl. Phys. A* **837** (2010) 65 [arXiv:0911.4806 [hep-ph]].
- [6] J. B. Kogut, M. A. Stephanov and D. Toublan, *Phys. Lett. B* **464** (1999) 183 [arXiv:hep-ph/9906346].
- [7] J. B. Kogut, M. A. Stephanov, D. Toublan, J. J. M. Verbaarschot and A. Zhitnitsky, *Nucl. Phys. B* **582** (2000) 477 [arXiv:hep-ph/0001171].
- [8] K. Splittorff, D. T. Son and M. A. Stephanov, *Phys. Rev. D* **64** (2001) 016003 [arXiv:hep-ph/0012274].
- [9] K. Splittorff, D. Toublan and J. J. M. Verbaarschot, *Nucl. Phys. B* **620** (2002) 290 [arXiv:hep-ph/0108040]; *ibid.* **639** (2002) 524 [arXiv:hep-ph/0204076].
- [10] G. V. Dunne and S. M. Nishigaki, *Nucl. Phys. B* **654** (2003) 445 [arXiv:hep-ph/0210219]; *ibid.* **670** (2003) 307 [arXiv:hep-ph/0306220].
- [11] T. Brauner, *Mod. Phys. Lett. A* **21**, 559 (2006) [arXiv:hep-ph/0601010].
- [12] T. Kanazawa, T. Wettig and N. Yamamoto, *JHEP* **0908** (2009) 003 [arXiv:0906.3579 [hep-ph]].
- [13] T. Kanazawa, T. Wettig and N. Yamamoto, *Phys. Rev. D* **81** (2010) 081701 [arXiv:0912.4999 [hep-ph]].
- [14] T. Kanazawa, T. Wettig and N. Yamamoto, *JHEP* **1112** (2011) 007 [arXiv:1110.5858 [hep-ph]].
- [15] A. Nakamura, *Phys. Lett. B* **149** (1984) 391.
- [16] S. Hands, J. B. Kogut, M. P. Lombardo and S. E. Morrison, *Nucl. Phys. B* **558** (1999) 327 [arXiv:hep-lat/9902034].
- [17] S. Hands, *et al.*, *Eur. Phys. J.* **C17** (2000) 285-302 [hep-lat/0006018]; S. Hands, I. Montvay, L. Scorzato, and J. Skullerud, *Eur. Phys. J.* **C22** (2001) 451-461 [hep-lat/0109029].
- [18] S. Muroya, A. Nakamura and C. Nonaka, *Nucl. Phys. Proc. Suppl.* **119** (2003) 544 [hep-lat/0208006].
- [19] S. Chandrasekharan and F. J. Jiang, *Phys. Rev. D* **74**, 014506 (2006) [arXiv:hep-lat/0602031].
- [20] S. Hands, S. Kim and J. I. Skullerud, *Eur. Phys. J. C* **48** (2006) 193 [arXiv:hep-lat/0604004].
- [21] S. Hands, S. Kim and J. I. Skullerud, *Phys. Rev. D* **81** (2010) 091502 [arXiv:1001.1682 [hep-lat]].
- [22] S. Hands, P. Kenny, S. Kim and J. I. Skullerud, *Eur. Phys. J. A* **47** (2011) 60 [arXiv:1101.4961 [hep-lat]].
- [23] L. A. Kondratyuk, M. M. Giannini and M. I. Krivoruchenko, *Phys. Lett. B* **269** (1991)

- 139.
- [24] L. A. Kondratyuk and M. I. Krivoruchenko, *Z. Phys. A* **344** (1992) 99.
- [25] R. Rapp, T. Schafer, E. V. Shuryak and M. Velkovsky, *Phys. Rev. Lett.* **81** (1998) 53 [hep-ph/9711396].
- [26] C. Ratti and W. Weise, *Phys. Rev. D* **70**, 054013 (2004) [arXiv:hep-ph/0406159].
- [27] G. Sun, L. He and P. Zhuang, *Phys. Rev. D* **75** (2007) 096004 [arXiv:hep-ph/0703159].
- [28] T. Brauner, K. Fukushima and Y. Hidaka, *Phys. Rev. D* **80**, 074035 (2009) [Erratum-ibid. *D* **81**, 119904 (2010)] [arXiv:0907.4905 [hep-ph]].
- [29] J. O. Andersen and T. Brauner, *Phys. Rev. D* **81** (2010) 096004 [arXiv:1001.5168 [hep-ph]].
- [30] M. Harada, C. Nonaka and T. Yamaoka, *Phys. Rev. D* **81** (2010) 096003 [arXiv:1002.4705 [hep-ph]].
- [31] T. Zhang, T. Brauner, D. H. Rischke, *JHEP* **1006** (2010) 064. [arXiv:1005.2928 [hep-ph]].
- [32] L. He, *Phys. Rev. D* **82** (2010) 096003 [arXiv:1007.1920 [hep-ph]].
- [33] P. de Forcrand, *PoS LAT2009* (2009) 010 [arXiv:1005.0539 [hep-lat]].
- [34] S. Diehl, S. Floerchinger, H. Gies, J. M. Pawłowski, C. Wetterich, *Annalen Phys.* **522** (2010) 615-656. [arXiv:0907.2193 [cond-mat.quant-gas]]; [35] M. M. Scherer, S. Floerchinger, H. Gies, [arXiv:1010.2890 [cond-mat.quant-gas]].
- [36] T. D. Cohen, *Phys. Rev. Lett.* **91** (2003) 222001 [arXiv:hep-ph/0307089]; T. D. Cohen, In \*Shifman, M. (ed.) et al.: From fields to strings, vol. 1\* 101-120 [hep-ph/0405043].
- [37] P. Braun-Munzinger, J. Stachel, *Nature* **448** (2007) 302-309.
- [38] A. Andronic, P. Braun-Munzinger, J. Stachel, *Phys. Lett.* **B673** (2009) 142-145. [arXiv:0812.1186 [nucl-th]].
- [39] L. -y. He, M. Jin, P. -f. Zhuang, *Phys. Rev.* **D71** (2005) 116001. [hep-ph/0503272].
- [40] J. Xiong, M. Jin, J. Li, *J. Phys. G* **G36** (2009) 125005.
- [41] K. Kamikado, N. Strodthoff, L. von Smekal, and J. Wambach, in preparation.
- [42] M. G. Alford, A. Schmitt, K. Rajagopal, T. Schafer, *Rev. Mod. Phys.* **80** (2008) 1455-1515. [arXiv:0709.4635 [hep-ph]].
- [43] A. W. Steiner, S. Reddy, M. Prakash, *Phys. Rev.* **D66** (2002) 094007. [hep-ph/0205201].
- [44] M. Huang, I. Shovkovy, *Nucl. Phys.* **A729** (2003) 835-863. [hep-ph/0307273].
- [45] M. Mitter, B. -J. Schaefer, N. Strodthoff, L. von Smekal, in preparation.
- [46] B. -J. Schaefer, J. M. Pawłowski, J. Wambach, *Phys. Rev.* **D76** (2007) 074023. [arXiv:0704.3234 [hep-ph]].
- [47] B. -J. Schaefer, M. Wagner, J. Wambach, *Phys. Rev.* **D81** (2010) 074013. [arXiv:0910.5628 [hep-ph]].
- [48] T. K. Herbst, J. M. Pawłowski, B. -J. Schaefer, *Phys. Lett.* **B696** (2011) 58-67. [arXiv:1008.0081 [hep-ph]].
- [49] J. Braun, H. Gies and J. M. Pawłowski, *Phys. Lett. B* **684** (2010) 262 [arXiv:0708.2413 [hep-th]].
- [50] F. Marhauser and J. M. Pawłowski, arXiv:0812.1144 [hep-ph].
- [51] V. Skokov, B. Friman, E. Nakano, K. Redlich and B. -J. Schaefer, *Phys. Rev. D* **82** (2010) 034029 [arXiv:1005.3166 [hep-ph]].
- [52] B. -J. Schaefer and M. Wagner, arXiv:1111.6871 [hep-ph].
- [53] O. Scavenius, A. Mocsy, I. N. Mishustin and D. H. Rischke, *Phys. Rev. C* **64** (2001) 045202 [arXiv:nucl-th/0007030].
- [54] A. Das, “*Finite Temperature Field Theory*,” World Scientific, Singapore (1997).
- [55] D. F. Litim and J. M. Pawłowski, arXiv:hep-th/9901063.
- [56] J. Berges, N. Tetradis, C. Wetterich, *Phys. Rept.* **363** (2002) 223-386. [hep-ph/0005122].
- [57] J. Polonyi, *Central Eur. J. Phys.* **1** (2003) 1 [hep-th/0110026].
- [58] J. M. Pawłowski, *Annals Phys.* **322** (2007) 2831-2915. [hep-th/0512261].
- [59] H. Gies, [hep-ph/0611146].
- [60] B. -J. Schaefer, J. Wambach, *Phys. Part. Nucl.* **39** (2008) 1025-1032. [hep-ph/0611191].
- [61] J. Braun, arXiv:1108.4449 [hep-ph].
- [62] C. Wetterich, *Phys. Lett.* **B301** (1993) 90-94.
- [63] D. F. Litim, *Phys. Rev.* **D64** (2001) 105007. [hep-th/0103195].
- [64] V. Skokov, B. Stokic, B. Friman and K. Redlich, *Phys. Rev. C* **82** (2010) 015206 [arXiv:1004.2665 [hep-ph]].
- [65] V. Skokov, B. Friman and K. Redlich, *Phys. Rev. C* **83**, 054904 (2011) [arXiv:1008.4570 [hep-ph]].
- [66] J. Braun, H. -J. Pirner and K. Schwenzer, *Phys. Rev. D* **70** (2004) 085016 [hep-ph/0312277].
- [67] B. J. Schaefer and J. Wambach, *Nucl. Phys. A* **757** (2005) 479 [arXiv:nucl-th/0403039].
- [68] J. Berges, D. U. Jungnickel and C. Wetterich, *Phys. Rev. D* **59** (1999) 034010 [arXiv:hep-ph/9705474].
- [69] B.-J. Schaefer and H.-J. Pirner, *Nucl. Phys. A* **660** (1999) 439 [arXiv:nucl-th/9903003].
- [70] O. Bohr, B. J. Schaefer and J. Wambach, *Int. J. Mod. Phys. A* **16** (2001) 3823 [arXiv:hep-ph/0007098].
- [71] B. Stokic, B. Friman and K. Redlich, *Eur. Phys. J. C* **67** (2010) 425 [arXiv:0904.0466 [hep-ph]].
- [72] J. Braun, B. Klein and P. Piasecki, *Eur. Phys. J. C* **71** (2011) 1576 [arXiv:1008.2155 [hep-ph]].
- [73] S. Holtmann, T. Schulze, *Phys. Rev.* **E68** (2003) 036111. [hep-lat/0305019].
- [74] D. F. Litim, *Nucl. Phys.* **B631** (2002) 128-158. [hep-th/0203006].
- [75] F. Benitez, J. -P. Blaizot, H. Chate, B. Delamotte, R. Mendez-Galain and N. Wschebor, arXiv:1110.2665 [cond-mat.stat-mech].
- [76] J. Braun, *Phys. Rev. D* **81** (2010) 016008 [arXiv:0908.1543 [hep-ph]].
- [77] E. E. Svanes and J. O. Andersen, *Nucl. Phys. A* **857** (2011) 16 [arXiv:1009.0430 [hep-ph]].
- [78] J. Braun, L. M. Haas, F. Marhauser and J. M. Pawłowski, *Phys. Rev. Lett.* **106** (2011) 022002 [arXiv:0908.0008 [hep-ph]].
- [79] J. M. Pawłowski, *AIP Conf. Proc.* **1343** (2011) 75 [arXiv:1012.5075 [hep-ph]].
- [80] D. F. Litim and D. Zappala, arXiv:1009.1948 [hep-th].
- [81] D. F. Litim and J. M. Pawłowski, *Phys. Lett. B* **546** (2002) 279 [arXiv:hep-th/0208216].
- [82] D. F. Litim and J. M. Pawłowski, *Phys. Lett. B* **516** (2001) 197 [arXiv:hep-th/0107020].
- [83] S. -B. Liao, *Phys. Rev.* **D53** (1996) 2020-2036. [hep-th/9501124].